MECHANISM OF DROPWISE CONDENSATION

Aydin Umur
Peter Griffith

May, 1963

Report No. 9041-25
Department of
Mechanical Engineering
Massachusetts Institute
of Technology

Contract No. NSF G-20947

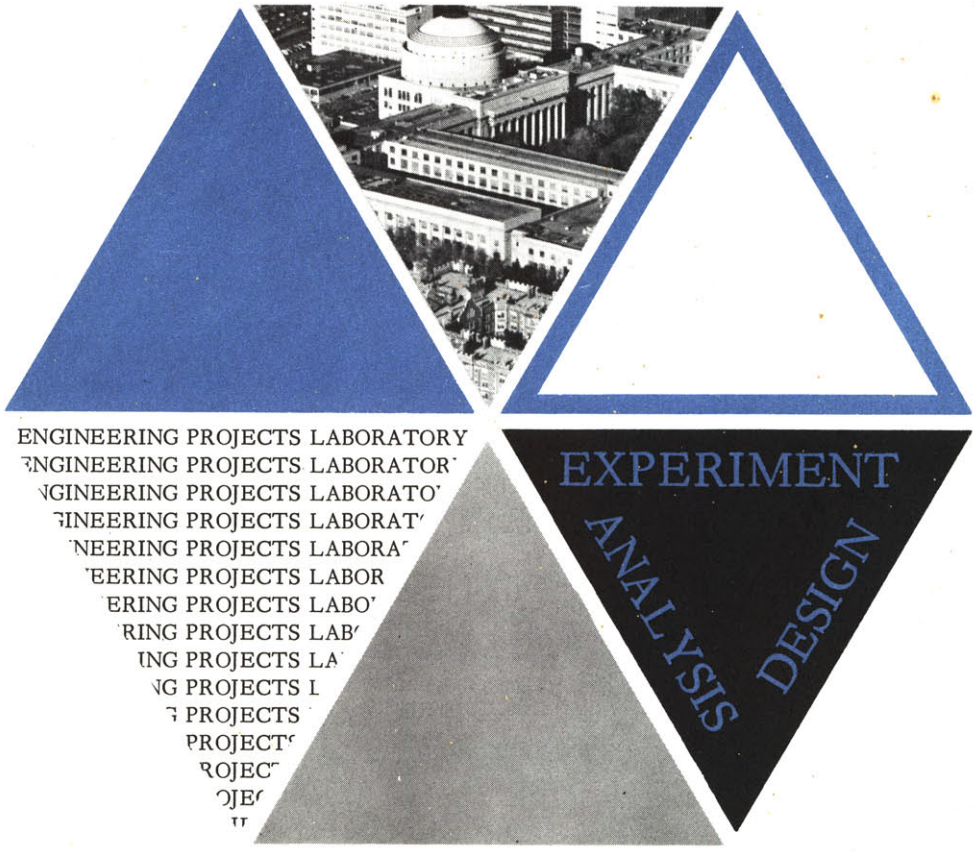

MECHANISM OF DROPWISE CONDENSATION

by

Aydin Umur
Peter Griffith

TECHNICAL REPORT NO. 9041-25

Sponsored by the
National Science Foundation
Contract No. NSF G-20947

Department of Mechanical Engineering
Massachusetts Institute of Technology
Cambridge 39, Massachusetts

ABSTRACT

From a study of surface phenomena, information is obtained about conditions under which net condensation can occur. An experimental examination of the surface, using an optical method capable of detecting thin films of molecular dimensions, shows that no film greater than a monolayer in thickness exists on the area between the drops. Wetted pits and grooves in the surface are considered to be the most probable drop nucleation sites. A model for drop growth gives results that are compatible with experimentally observed values, and show the growth rate to be a function of the vapor pressure.

TABLE OF CONTENTS

1. INTRODUCTION

Most pure vapors condense on clean surfaces in the form of a continuous film. If, however, the surface is contaminated, particularly with fatty acids, dropwise condensation may occur. On examining such a surface, tiny droplets are seen to appear, grow, and coalesce with one another until a large drop rolls off the surface, sweeping along with it drops that lie in its path; on the strip of area cleared in this manner, new droplets form. With this type of condensation, heat transfer coefficients are observed to be much higher than with film condensation. This increase in the heat transfer is the cause of the considerable interest in the subject. Recent advances in the use of promoters[3,4,18,25,28] make it possible to achieve dropwise condensation of long duration and high dependability.

A basic understanding of the mechanism of dropwise condensation requires a knowledge of how the drops form and grow. Jakob[12] proposed that a very thin layer of "steam or water" rapidly develops on the surface, breaking into droplets after a certain thickness is reached; a new film immediately appears over the exposed area. This would explain the high heat transfer coefficients observed, since condensation would be taking place on a thin film having a low resistance to heat transfer. Jakob's view was later supported by Baer and McKelvey[2]; and Welch and Westwater[28] presented a sequence of photographs taken through a microscope showing that the area cleared when two drops coalesce on a copper surface first has a shiny appearance, but very quickly becomes dull, suggesting the formation of a film.

Tammann and Boehme[24], on the other hand, observed that upon repetitive

condensation drops appear to have the same arrangement on the surface, suggesting the existence of particular nucleation sites. This observation was substantiated recently by McCormick and Baer[17,16] who have studied drop formation and growth under carefully controlled experimental conditions. Their results indicate that drops nucleate from randomly distributed sites, and that these sites are probably pits and grooves in the surface. The authors consider it unlikely that any condensation is taking place between the drops, and propose a mechanism based on the assumption that heat is being transferred by conduction through the drops.

Whether or not net condensation takes place on the area between the drops has not been clear. Eucken[7] proposed that liquid nucleation occurs in a thin layer of supersaturated vapor next to the surface, and that in this layer there is a flow toward the drops because of a density gradient created by condensation on the surface of the drops. Emmons[6], on the other hand, considered the area between the drops as being bare.

Other aspects of dropwise condensation have been examined by various investigators. Gnam's experiments[10] stress the cyclic nature of dropwise condensation, and show the effect of vapor pressure on the heat transfer coefficient. Hampson and Ozisik[11] have studied drop size and distribution, and point out the regularity in the pattern of drop growth within the cyclic period. Fatica and Katz[8], and Sugawara and Michiyoshi[23] have obtained semi-quantitative expressions for the heat transfer coefficient.

In the present investigation, conditions for net condensation are examined from the point of view of surface phenomena. The surface is observed experimentally using an optical method capable of detecting film thicknesses of molecular dimensions. In the light of information obtained in this manner, drop nucleation and the growth of individual drops are analyzed.

2. SURFACE PHENOMENA ASSOCIATED WITH CONDENSATION

2.1 Adsorbtion on Surfaces

In his studies on the adsorbtion of gases and vapors, Langmuir [14, 15] postulated that nearly all molecules that strike a surface condense on the surface and subsequently evaporate. Here the term condense has the meaning that the molecule is caught in the surface force field and becomes attached to the surface. Evaporation occurs when the molecule frees itself from the surface. Under steady state conditions condensation and evaporation rates are equal, and there exist on the surface an average number of adsorbed molecules.

From kinetic theory, the rate of condensation on a surface per unit area can be expressed as

$$w_+ = \gamma P_v \left(\frac{g}{2\pi R T_v}\right)^{1/2} \tag{1}$$

where P_v and T_v are the pressure and temperature of the vapor, respectively, R is the gas constant, g is the gravitational constant, and γ is the condensation coefficient (fraction of molecules that strike the surface that condense). Rate of evaporation from the surface per unit area can be expressed in the form of a Boltzmann law

$$w_- = w_o f_s e^{-\frac{\lambda_s}{R T_s}} \tag{2}$$

where w_o is a proportionality constant, f_s is the fraction of the surface covered with adsorbed molecules, λ_s is the energy per unit mass required to evaporate the adsorbed molecules, and T_s is the surface temperature.

2.2 Equilibrium Between Saturated Vapor and Solid Surface

Fig. 1 represents a system consisting of a vapor, its liquid phase, and a solid surface. At equilibrium the vapor is saturated and the temperature is uniform throughout the system. Also, condensation and evaporation rates are equal both at the liquid-vapor interface and at the solid surface, so that

$$w_{l+} = w_{l-} \quad ; \quad w_{s+} = w_{s-}$$

Using Eq. 1

$$\frac{w_{l+}}{\gamma_l} = P_v \left(\frac{g}{2\pi RT}\right) = \frac{w_{s+}}{\gamma_s}$$

Therefore

$$\frac{w_{l-}}{\gamma_l} = \frac{w_{s-}}{\gamma_s}$$

and with the use of Eq. 2

$$f_s = \frac{\gamma_s}{\gamma_l} e^{\frac{\lambda_l}{RT}\left(\frac{\lambda_s}{\lambda_l} - 1\right)} \tag{3}$$

where the subscript s refers to the solid surface, and the subscript ℓ to the liquid-vapor interface. Eq. 3 gives information about the condition of a solid surface exposed to a saturated vapor with which it is in equilibrium. Two distinct cases are apparent depending on whether the ratio of the evaporation energies λ_s / λ_ℓ is greater or less than unity. In the former case, f_s is greater than unity+, and the surface must be covered with more than a complete monolayer. In fact, Eq. 3 is satisfied only when there exist on the surface a sufficiently large number of layers so that the outermost layer can be considered a true liquid phase. The evaporation energy then becomes identical to the evaporation energy from the liquid-vapor interface, and Eq. 3 gives a value of f_s equal to unity.

When λ_s / λ_ℓ is less than unity, f_s is less than unity, indicating that in this case there can be no more than an incomplete monolayer on the solid surface.

2.3 Evaporation Energies and Contact Angle

There is a simple approximate relation between the ratio of the evaporation energies λ_s / λ_ℓ and the contact angle θ (Fig. 2). The work of adhesion per unit area of contact between the liquid and the solid, i.e. the energy required to separate the two, can be expressed in terms of the surface energies per unit area

$$W_{s\ell} = \sigma_{sv} + \sigma_{\ell v} - \sigma_{s\ell}$$

+When λ_s / λ_ℓ is greater than unity, the ratio of the condensation coefficients γ_s / γ_ℓ is also greater than unity. This is because in this case the solid surface must have a stronger force field than the liquid-vapor interface, and therefore attracts a greater number of vapor molecules.

where σ_{sv} and σ_{lv} are the surface energies of the two new interfaces that are formed by the separation, and σ_{sl} is the surface energy of the original interface. From Fig. 2

$$\sigma_{sv} = \sigma_{sl} + \sigma_{lv} \cos\theta$$

Combining the two equations above

$$W_{sl} = \sigma_{lv} (1 + \cos\theta)$$

On the other hand, work of cohesion within the liquid itself, defined as the energy required to break a column of liquid of unit cross section, is given by

$$W_{ll} = 2\,\sigma_{lv}$$

since two interfaces are formed where none existed originally. Finally

$$\frac{\lambda_s}{\lambda_l} \approx \frac{W_{sl}}{W_{ll}} = \frac{1}{2}(1 + \cos\theta) \qquad (4)$$

Eq. 4 shows that when θ is zero, λ_s/λ_l is unity. For any value of θ greater than zero (non-spreading liquid), λ_s/λ_l is less than unity. Whereas, λ_s/λ_l is greater than unity only when the liquid spreads on the surface.

2.4 Conditions for Equilibrium when Vapor is not Saturated

It is desirable to examine the more general case of a solid exposed to a vapor which may be superheated or supersaturated. The temperature of the system is still assumed to be uniform. Frenkel[9] gives an expression for the Gibbs potential of a system consisting of a vapor and a thin film on a surface of unit area, as a function of the film thickness. A derivation is given in Appendix A. The result is

$$Z = \frac{\zeta_l - \zeta_v}{v_l}\delta + \frac{\lambda_s - \lambda_l}{2v_l}\frac{\mu^3}{\delta^2} + \left[\frac{(3\lambda_l - \lambda_s)\mu}{2v_l} + \zeta_v M\right] \qquad (5)$$

where ζ_l and ζ_v are the Gibbs potentials per unit mass of the liquid and the vapor, respectively, v_l is the specific volume of the liquid, δ is the film thickness, μ is the molecular diameter, and M is the total mass contained in the system. The variation of the Gibbs potential Z with film thickness δ is indicated in Fig. 3. From thermodynamics, minimum values of Z correspond to stable equilibrium states, whereas maximum values of Z correspond to unstable equilibrium states. Furthermore, any spontaneous change in the state of the system is toward a lower value of Z. Fig. 3 shows that in the case of a spreading liquid, stable equilibrium states occur when the vapor is superheated. Since for any given state of superheat the thickness of the adsorbed layer must correspond to the minimum value of the Gibbs potential, more and more molecules are adsorbed on the surface as the vapor state is changed toward saturation. At saturation the adsorbed layer becomes infinitely thick (true liquid phase), and with any amount of supersaturation net condensation occurs. This behaviour has been verified experimentally by Derjaguin and

Zorin[5] who measured the thickness of the adsorbed layer as a function of the vapor state as saturation was approached. Water vapor was among the substances they used. The surface was clean glass.

With a non-spreading liquid, however, the equilibrium states, which occur when the vapor is supersaturated, are unstable. For any given state of supersaturation there is a corresponding critical film thickness δ^* which must be exceeded if there is to be net condensation. Any film with a thickness smaller than δ^* evaporates until there is less than a monolayer left on the surface.

Information about the equilibrium states can be obtained from

$$\frac{\partial Z}{\partial \delta} = 0$$

which, with the use of Eq. 5, gives

$$\ln \frac{P_\delta^{**}}{P^*} = \frac{\lambda_l}{RT}\left(1 - \frac{\lambda_s}{\lambda_l}\right)\left(\frac{\mu}{\delta}\right)^3 \qquad (6)$$

where P_δ^{**} is the equilibrium pressure corresponding to a film thickness δ, and P^* is the saturation pressure corresponding to the uniform temperature T of the system.

2.5 Effect of Lowering Surface Temperature

When the surface is at a lower temperature than the vapor, there can be no thermodynamic equilibrium because of the non-uniformity in the temperature of the system. The equilibrium film thickness of the previous section is now defined, without altering its significance, as the thickness δ_o at which there is no net mass transfer across the film-vapor interface.

Schrage[21] used kinetic theory to arrive at an expression for inter-phase mass transfer under non-equilibrium conditions. The following is a slightly modified form[22] of Schrage's equation

$$w = \left(\frac{2\gamma}{2-\gamma}\right)\left(\frac{g}{2\pi R}\right)^{1/2}\left[\frac{P_v}{T_v^{1/2}} - \frac{P_i^{**}}{T_i^{1/2}}\right] \tag{7}$$

where w is the net rate of condensation per unit area of the interface, and P_i^{**} is the equilibrium pressure corresponding to the interface temperature T_i. Since the interface in this case is between a thin film and a vapor, the value for P_i^{**} may be substituted from Eq. 6 after replacing P^{**} in that equation by P_i^{**}, P^* by P_i^*, and T by T_i. The result is

$$w = \left(\frac{2\gamma}{2-\gamma}\right)\left(\frac{g}{2\pi R}\right)^{1/2}\left[\frac{P_v}{T_v^{1/2}} - \frac{P_i^*}{T_i^{1/2}}\, e^{\frac{\lambda_l}{RT_i}\left(1-\frac{\lambda_s}{\lambda_l}\right)\left(\frac{\mu}{\delta}\right)^3}\right] \tag{8}$$

An expression for δ_o can be found by setting Eq. 8 equal to zero.

If as a special case saturated vapor is considered, the resulting equation simplifies to

$$\frac{\delta_o}{\mu} = \left[\frac{1 - \frac{\lambda_s}{\lambda_l}}{1 - \frac{T_i}{T_v}\left(1 + \frac{RT_v}{2\lambda_l} \ln \frac{T_v}{T_i}\right)} \right]^{1/3} \qquad (9)$$

Since the film thicknesses involved are extremely small, the interface temperature T_i in Eq. 9 is virtually the same as the surface temperature T_s. The variation of δ_o as the surface temperature is decreased is indicated in Fig. 4. If changing the surface temperature is considered as changing the relative superheat or supersaturation of the vapor, Fig. 4 is seen to be the equivalent of Fig. 3.

2.6 Summary

The theoretical considerations presented in this chapter indicate that in the case of a non-spreading liquid, which is the case for dropwise condensation, a thin film cannot spontaneously develop on the surface even with large relative supersaturation of the vapor. For net condensation to occur, the film must have a thickness larger than a critical thickness corresponding to the degree of relative supersaturation of the vapor. Any film smaller than this thickness evaporates until less than a monolayer is left on the surface.

The estimated critical thickness for water vapor saturated at atmospheric pressure and with a wall subcooling of 0.1°F is 14 molecular

layers. With 1°F the critical thickness is 6 molecular layers, and with 10°F it is 3 molecular layers.

3. EXPERIMENTAL INVESTIGATION

3.1 Optical Measurement of Thin Films+

It is known from electromagnetic theory that when plane polarized light is incident on a clean metallic surface, the reflected light is elliptically polarized. The formation of a thin transparent film on the surface causes a change in the ellipticity by an amount which is a function of the film thickness. In Fig. 5a, the reflected light is seen to be a combination of the reflections from the outer surface of the film and the metal base. The part of the light that travels through the film suffers a phase retardation proportional to the optical distance travelled. Fig. 5b represents the polarization of the reflected light. R_p and R_s are the components of the electric vector parallel and perpendicular, respectively, to the plane of incidence. They are out of phase with respect to one another by an angle Δ (not shown in figure). Angle ψ is defined by

$$\tan \psi = \frac{R_p}{R_s} \quad ,$$

α is the orientation angle of the ellipse, and β is the ellipticity angle.

A method of determining the film thickness δ consists of measuring α and β experimentally, then calculating δ by using known theoretical

---

+For a theoretical treatment of optics of thin films see Vasicek[27].

relations. This method has been used successfully by a number of investigators[5,20,26] to measure thin films having thicknesses ranging from 1A to 1000A.

3.2 Optical Method used in Present Investigation

Measuring the orientation and the ellipticity angles, α and β, of the light reflected from the surface involves making adjustments in the optical system. The method outlined in the previous section is therefore not suitable for a continuous observation of the surface.

In Fig. 6, the dotted ellipse, with orientation angle α_o, represents the polarization of light reflected from a surface having no film (dry metal). With a film of thickness δ the ellipse changes as shown, so that the orientation angle becomes α. Considering this new ellipse, the following relationship is derived in Appendix B

$$\frac{I_m}{I_t} = \frac{1}{2}\left[1 - \cos 2\beta \cos 2(\alpha_o - \alpha)\right] \qquad (10)$$

where I_m is the intensity of light along the initial minor axis, and I_t is the total intensity of the reflected light. For a given set of conditions, it is possible to calculate α_o, α, β, and I_t as a function of δ. δ is then related to I_m through Eq. 10. The appropriate equations to be used to obtain this relation, together with a numerical example, are given in Appendix C. The advantage of this procedure is that since I_m is always measured in the same plane, changes in the film thickness δ can be observed continuously after making an

initial adjustment in the optical apparatus.

3.3 Experimental Arrangement and Testing Procedure

Arrangement of the experimental apparatus is shown in Fig. 7. Saturated steam at atmospheric pressure was supplied to the test chamber and to the outer chamber, the latter serving as thermal insulation. Promoter, when used, was added to the water in the boiler. Condensates from the two chambers were discarded. Light was reflected from the polished surface of a rectangular copper bar (later gold plated) held in a vertical position with the lower end extending into the lower chamber. Cooling water at a controlled temperature was pumped through the lower chamber. The reason for this cooling arrangement was to obtain small temperature differences between the vapor and the test surface, and to facilitate measurement of the surface temperature by having horizontal sections of the bar nearly uniform in temperature. The test chamber and the test surface are seen in greater detail in Fig. 8. Steam temperature and the temperature of the surface at three different elevations were measured with copper-constantan thermocouples. The thermocouples were installed in the copper bar in horizontal planes with the junctions close to the test surface.

Fig.8 also shows the optical arrangement. On the incident side (left), a light source, a filter (5461Å), a pinhole, a polarizer (nicol prism), and a lens are seen in that order. The light then passes through a window into the test chamber, and is focused on the test surface on an elliptical area about 1 mm high and 2 mm wide. The reflected light passes through another window, a lens, a quarter-wave plate, an analyzer (nicol prism), another lens, finally falling on the cathode of a photomultiplier

tube. The output of the photomultiplier tube is amplified and continuously recorded. The light source used was a concentrated tungsten filament projection lamp, and was found to have a minimum amount of fluctuations in light intensity among the light sources considered. The various lenses were used for focusing the light. The two windows were made of flat rectangular pieces of electrically conducting glass, and were heated to keep them free from vapor condensation. It was noticed that the light passing through the windows was slightly altered, apparently due to thermal stresses in the glass; but the magnitude of this alteration was not enough to have an appreciable effect on the measurements.

In a typical run, steam was introduced into the outer chamber and the test chamber, and the cooling water circulation was started. After steady state was established with dropwise condensation taking place, the test surface was heated electrically to a temperature up to 10°F higher than the steam temperature. The surface was considered to be completely dry under these conditions, and the reflected light was analyzed to determine α_o and β_o by using the quarter-wave plate and the analyzer in a standard manner. The quarter-wave plate was then removed from the system, and the analyzer was set to a position allowing only the light along the minor axis of the ellipse to pass through. While the intensity of this light was continuously recorded, and without altering the position of the analyzer, the surface temperature was lowered either by shutting off the surface heater completely, or by reducing the power input of the heater in steps. The run was continued until the initial steady state conditions, with dropwise condensation taking place on the surface, were reached. The variation in the light intensity was then examined. From theory, an increase in light intensity indicates an increasing film thickness (see Fig. 11). With the formation of drops, however, a reduction

in the intensity is expected since the light falling on the drops is scattered.

3.4 Results

Initially, a copper surface was used with cupric oleate added to the boiling water as promoter. Two difficulties were encountered. First, non-uniform oxidation of the copper surface, when it was exposed to the promoted steam, changed the optical properties of the surface in an unpredictable manner so that accurate calculations were not possible. Second, the promoter molecules in the steam were condensing on the surface and forming a film of their own, making it difficult to differentiate whether any film observed was a film of cupric oleate or water. Fig. 9a represents a typical result obtained with the copper surface. It is seen that as the surface temperature starts to fall after the surface heater is shut off, there is a substantial increase in the intensity, indicating an increasing film thickness. The intensity falls as soon as drops form on the surface. A rough estimate indicated that the total increase in the film thickness (until the appearance of the drops) was about 25Å. The fluctuations shown in the figure, amounting to about $\pm 1\ \%$, correspond to similar fluctuations in the film thickness, and were not inherent in the optical system. When, for example, the analyzer was removed so that the total light intensity was recorded, the fluctuations disappeared. There is little doubt therefore, that a fairly volatile film of promoter molecules was present on the surface even when the surface temperature was well above the temperature of the vapor. The increase in film thickness as the surface temperature was lowered may well have been

due to a greater accumulation of promoter molecules on the surface.

To eliminate the complication of an oxide layer, the copper surface was gold plated. On the gold surface, perfect dropwise condensation occurred without the introduction of a promoter into the system, apparently because of contamination of the surface from the air. Since low condensation ~~of~~ rates were used, and they were of short duration, condensation on the surface remained dropwise. In this way, the complication caused by excessive promoter molecules was also eliminated. A typical result obtained with the gold surface is indicated in Fig. 9b. In this case, no significant increase in the light intensity was observed. For the set of conditions used, a monolayer of water molecules would have caused an increase in intensity of a little less than 1%. A 1% increase would have been easily observable. It was therefore concluded that no film more than a monolayer in thickness existed on the surface. On numerous occasions, after the appearance of drops on the surface the test area was momentarily cleared by a rolling drop, and the light intensity rapidly increased to its initial value; but did not at any time exceed this value. This indicates that the rolling drops did not leave thin films behind them.

Most of the runs were made with a surface subcooling, at steady state, of about 0.01°F. In a few cases, however, the subcooling was increased up to about 0.5°F. Runs were also made at different angles of incidence of light, and using different test areas on the surface. In all cases, the results were essentially the same.

3.5 Accuracy of the Optical System

The performance of the optical system was checked in several ways. The thickness of the oxide layer on the copper surface (soon after the

surface was polished) was measured by using the method of Section 3.1. A thickness of about 50Å was determined, which is a reasonable value. The optical constants (index of refraction and absorbtion index) of the gold surface were determined at two different angles of incidence. The results showed very good agreement with values reported in the literature.

To check the method of Section 3.2, a small quantity of alcohol was injected on the gold surface. Since alcohol spreads on gold, a film was formed. The thickness of this film decreased with time mostly by a downward flow of the liquid, and also by evaporation. The change in the thickness was measured by recording the light intensity I_m. Fig. 10 shows the variation of I_m with time, and may be compared to Fig. 11 where the calculated value of I_m is plotted against the film thickness δ. As can be seen, I_m undergoes cyclic changes each cycle corresponding to 2500Å. The reason for the initial damping in the experimental value is that the film thickness is not uniform over the test area, and at any given time an average thickness is measured. As the film becomes thinner the non-uniformity decreases, and the average thickness follows the theoretical curve more closely.

3.6 Discussion

The experiments show that no film greater than a monolayer in thickness forms on the surface as the surface temperature is cooled to below the vapor temperature. This is in agreement with the theoretical results of Chapter 2, where an examination of surface phenomena indicated that with a non-spreading liquid a film cannot spontaneously develop on the surface. The mechanism that drops are formed from a film developing on the surface is, therefore, incorrect. Individual nucleation of the

drops remains as the other alternative.

The theoretical results indicate that if a film having a thickness greater than a certain critical thickness does exist on the surface, then net condensation occurs on this film. But since such a film cannot form by itself, if it exists at all, it must be introduced by some other means. One conceivable way for this to happen in dropwise condensation is that the drops, as they roll over the surface, might leave a film behind them. The experiments show, however, that this does not happen; rolling drops leave behind them at most a monolayer. It can be concluded, therefore, that no film greater than a monolayer in thickness exists on the area between the drops, and that no net condensation takes place on this area. Compared to the energy released by condensation, any amount of heat transfer by convection is negligible. With a wall subcooling of 10°F, for example, the maximum amount of heat transfer by convection is about 5 Btu per pound of steam; whereas for every pound of steam that condenses on the drops about 1000 Btu of energy is released. Consequently, nearly all the energy transferred to the wall must be transferred through the drops.

These considerations lead to a closer examination of the drop nucleation process, and the rate of growth of the drops.

4. DROP NUCLEATION AND GROWTH

4.1 Nucleation

Results of Chapter 2 indicate that in the case of a non-spreading liquid, adsorbed molecules on a surface are restricted to less than a monolayer even when the surface is subcooled to below the vapor saturation temperature. If, however, there exist on the surface particular areas on which the liquid spreads, then on these areas net condensation occurs with any amount of relative supersaturation of the vapor. When the liquid, accumulated in this fashion, establishes the proper contact angle with the rest of the surface a drop is formed. Whether or not such a drop will continue to grow depends on the conditions for thermodynamic equilibrium of a drop. The critical radius r^*, representing drop size at which there is unstable equilibrium between the drop and the surrounding vapor, can be determined from the Kelvin-Helmholtz equation[13]

$$\ln \frac{P_r^{**}}{P^*} = \frac{2\sigma V_\ell}{rRT} \qquad (12)$$

where P_r^{**} is the equilibrium pressure corresponding to the drop radius r, P^* is the saturation pressure corresponding to the uniform temperature T of the system, σ is the surface tension, V_ℓ is the specific volume of the liquid, and R is the gas constant. If P_r^{**} is interpreted as the actual pressure of the vapor, then r is the critical radius r^* corresponding to that pressure. In order for a drop to grow, its radius must be larger than the critical radius.

In the dropwise condensation of steam, faults in the promotion may result in areas that satisfy the spreading condition. On a smooth surface, the size of these areas would have to be very large in terms of molecular dimensions so that drops larger than the critical size may form. It is considered far more likely that much smaller unpromoted areas exist inside pits and grooves in the surface. In this case, depending on the particular geometry, very small quantities of liquid would be sufficient for drop nucleation. If, for example, a conical pit of semi-cone angle ψ_c is considered, the necessary and sufficient conditions for drop nucleation become

1. $D > 2r^* \sin \theta$, where D is the mouth diameter of the pit and θ is the contact angle.

2. Either $\theta + \psi_c \leq 90°$ and a sufficient number of molecules are present in the pit to constitute a true liquid phase; or $\theta + \psi_c > 90°$ and enough liquid is present in the pit such that

$$l > r^* \frac{\sin(\theta + \psi_c - 90°)}{\sin \psi_c}$$

where l is the lateral height of liquid that must be present in the pit.

These two conditions ensure that the radius of curvature r of the liquid-vapor interface is always greater than r^* (or else it is negative so that the interface is concave). The nucleation period is complete when the liquid reaches the top of the pit, and a drop making the proper contact angle with the surface is established.

4.2 Growth of Hemispherical Drops

The analysis in this section is restricted to hemispherical drops. In a later section contact angles other than 90° will be considered. Fig 12 shows the model used. Heat transfer from the vapor to the drop is assumed to be negligible compared to the transport of energy as a result of condensation. At the liquid-vapor interface an equivalent heat transfer coefficient h_e is used, which, as will be seen later, is virtually independent of ϕ. The base of the drop is assumed to be at a uniform temperature. It is further assumed that heat transfer through the drop is by conduction alone.

The steady state conduction equation

$$\frac{\partial}{\partial \rho}\left(\rho^2 \frac{\partial T}{\partial \rho}\right) + \frac{1}{\sin\phi}\,\frac{\partial}{\partial \phi}\left(\sin\phi\,\frac{\partial T}{\partial \phi}\right) = 0$$

with the boundary conditions

$$T\left(\rho, \pm\frac{\pi}{2}\right) = T_s$$

$$T(0, \phi) \neq \infty$$

$$\frac{\partial}{\partial \rho} T(r, \phi) = \frac{h_e}{k_l}\left[T_i - T(r, \phi)\right]$$

has the solution

$$\frac{T(\rho,\phi)-T_s}{T_v-T_s} = \sum_{\substack{m=1\\ \text{odd}}}^{\infty} \left[\frac{2m+1}{1+\frac{k_\ell}{h_e r}m} \int_0^1 P_m(x)\,dx\right]\left(\frac{\rho}{r}\right)^m P_m(\cos\phi) \qquad (13)$$

where k_ℓ is the thermal conductivity of the liquid, and P_m are Legendre polynomials of the first kind. At $\rho = r$ Eq. 13 gives the temperature of the liquid-vapor interface T_i as a function of ϕ. The average temperature over the area of the interface T_{ia} is found to be

$$\frac{T_{ia}-T_s}{T_v-T_s} = \sum_{\substack{m=1\\ \text{odd}}}^{\infty} \frac{2m+1}{1+\frac{k_\ell}{h_e r}m} \left[\int_0^1 P_m(x)\,dx\right]^2 \qquad (14)$$

The rate of heat transfer through the drop can be determined from

$$q_d = 2\pi r^2 k_\ell \int_0^{\frac{\pi}{2}} \frac{\partial}{\partial \rho} T(r,\phi) \sin\phi\, d\phi$$

Using Eq. 13

$$q_d = 2\pi r k_\ell (T_v-T_s) \sum_{\substack{m=1\\ \text{odd}}}^{\infty} \frac{m(2m+1)}{1+\frac{k_\ell}{h_e r}m} \left[\int_0^1 P_m(x)dx\right]^2 \qquad (15)$$

The total energy transferred to a drop of radius r may be expressed as

$$Q = \rho_\ell V \lambda = \frac{2}{3} \pi \rho_\ell \lambda r^3$$

where ρ_ℓ is the density of the liquid, V is the volume of the drop, and λ is the latent heat of vaporization. Differentiating with respect to time

$$\frac{dQ}{dt} = q_d = 2\pi \rho_\ell \lambda r^2 \frac{dr}{dt} \tag{16}$$

Eqs. 15 and 16 may be combined to give the drop growth rate

$$\frac{dr}{dt} = \frac{k_\ell (T_v - T_s)}{\rho_\ell \lambda r} \sum_{\substack{m=1 \\ \text{odd}}}^{\infty} \frac{m(2m+1)}{1 + \frac{k_\ell}{h_e r} m} \left[\int_0^1 P_m(x)\, dx \right]^2 \tag{17}$$

Using Eqs. 14, 15, and 17, the dimensionless groups

$$\frac{T_{ia} - T_s}{T_v - T_s} \quad , \quad \frac{q_d}{r k_\ell (T_v - T_s)} \quad , \quad \frac{\rho_\ell \lambda r}{k_\ell (T_v - T_s)} \frac{dr}{dt}$$

are plotted against $k_\ell / h_e r$ in Fig. 13.

An expression for h_e may be obtained by starting with Eq. 7 of section 2.5, which, with the use of Eq. 12 of Section 4.1, becomes the net condensation rate on a drop of radius r

$$w = \left(\frac{2\gamma}{2-\gamma}\right)\left(\frac{g}{2\pi R}\right)^{1/2} \frac{P_v}{T_v^{1/2}} \left[1 - \frac{P_i^*}{P_v} e^{\frac{2\sigma v_\ell}{rRT_i}}\right] \qquad (18)$$

If it is assumed that the vapor is saturated, P_v in Eq. 18 becomes the saturation pressure P_v^*.

Using

$$\ln \frac{P_i^*}{P_v^*} = -\frac{\lambda}{RT_i}\left(1 - \frac{T_i}{T_v}\right)$$

which follows from the Clausius-Clapeyron relation, the term inside the bracket in Eq. 18 becomes

$$1 - e^{-\frac{\lambda}{RT_i}\left(1-\frac{T_i}{T_v}\right)\left[1-\frac{2\sigma v_\ell}{r\lambda\left(1-\frac{T_i}{T_v}\right)}\right]} = 1 - e^{-\frac{\lambda}{RT_i}\left(1-\frac{T_i}{T_v}\right)\left(1-\frac{r^*}{r}\right)}$$

where r^* is the critical radius. For water, λ/RT_i is close to 10, and T_i/T_v is rarely smaller than 0.99. Therefore

$$\frac{\lambda}{RT_i}\left(1-\frac{T_i}{T_v}\right)\left(1-\frac{r^*}{r}\right) < 0.1$$

Noting that

$$1 - e^{-x} = x - \frac{x^2}{2!} + \frac{x^3}{3!} - \cdots \approx x \quad , \quad x < 0.1$$

the condensation rate may be expressed as

$$w \approx \left(\frac{2\gamma}{2-\gamma}\right)\left(\frac{g}{2\pi}\right)^{1/2} \frac{\lambda P_v^*}{R^{3/2} T_v^{5/2}} \left(1 - \frac{r^*}{r}\right)\left(T_v - T_i\right) \qquad (19)$$

with an error of less than 5%. In obtaining Eq. 19 the substitution

$$T_v^{3/2} T_i \approx T_v^{5/2}$$

was used. The resulting error is negligible. An expression for h_e is therefore

$$h_e \equiv \frac{w\lambda}{T_v - T_i} = \left(\frac{2\gamma}{2-\gamma}\right)\left(\frac{g}{2\pi}\right)^{1/2} \frac{\lambda^2 P_v^*}{R^{3/2} T_v^{5/2}} \left(1 - \frac{r^*}{r}\right) \qquad (20)$$

It should be noted that the liquid-vapor interface temperature T_i does not appear on the right hand side of Eq. 20 except through r^*, which is a function of $(T_V - T_i)$. However, when $r = r^*$, h_e is zero; and as the drop radius increases, the dependence of r^* on the interface temperature has little effect on the value of h_e. The assertion that was made earlier that h_e is virtually independent of ϕ is therefore justified.

The condensation coefficient γ appearing in Eq. 20 has been determined

for water by Pruger[19] and by Alty and Mackay [1]. The values they report are 0.04 and 0.036, respectively. However, Silver and Simpson[22] report a value of 0.003, and suggest that γ might be a function of temperature. They also state that no special precaution was taken to purify the water used in their experimentation, and that the low value obtained might therefore be due to surface contamination. In calculations that follow, γ was taken to be 0.04 with the understanding that h_e is significantly effected by large changes in γ.

With the use of Eqs. 17 and 20 drop size may be determined as a function of time for a given vapor state and wall subcooling. The procedure is first to determine dr/dt as a function of r, and then integrate numerically between the limits t = 0, r = r_o, and t,r. Here r_o represents the size of a newly formed drop and must have a value greater than r^*.

McCormick and Baer[17] have observed drop growth experimentally by using very small wall subcooling to slow the process down, and taking photographs of the surface at convenient time intervals under high magnification. Saturated steam at room temperature was used. The degree of wall subcooling was not measured because of its small magnitude. Fig. 14 is a reproduction of their result . Each set of points belong to a different drop on the same surface and appears to fall along a straight line. By assuming that the liquid-vapor interface is at the vapor temperature, the authors estimate the wall subcooling from the slope of the lines and obtain a value of about 0.001°F. A difficulty arises when it is noted that all the drops represented in Fig. 14 are considerably smaller than the critical drop size ($r^* \approx$ 30 microns) corresponding to 0.001°F subcooling.

Since every drop has a different history of formation, nucleation time will vary from drop to drop. When each set of points in Fig. 14

is shifted along the time axis all the points fall approximately on the same line, as shown in Fig. 15. Calculations using Eqs. 17 and 20 (with r_o taken as 5 microns) indicate that the data correspond to a wall subcooling of about 0.012°F. The critical radius for this subcooling is 2.33 microns, so that the smallest drop observed is about 2.5 times the critical size. This may also explain why the three lowest points in Fig. 15 are off the curve; the drops represented by these points are close to the critical size and may still be in the nucleation stage.

4.3 Effect of Vapor Pressure

From Eq. 20

$$h_e \sim \frac{P_v^*}{T_v^{5/2}}$$

where T_v is expressed on the absolute temperature scale, so that lowering the saturation pressure causes a significant decrease in h_e. As a result, the drop growth rate will also decrease, as can be seen from Eq. 17.

Fig. 16 illustrates the effect of pressure on drop growth. Drop size is plotted against time for three different pressures for a wall subcooling of 1°F. The time scale starts at r_o= 0.1 micron, about three times the critical radius. The differences in drop growth rate are seen to be substantial. As an example, a radius of 10 microns (D^2 = 400) is reached in about 0.3 seconds at atmospheric pressure, 0.7 seconds at a pressure of 2.89 psia, and 3 seconds at 0.363 psia. The dotted line in the figure indicates the rate at which a drop would grow if the liquid-vapor interface were at the vapor temperature. It is interesting to note that if this were the case a 10 micron radius would have been reached in about 0.05 seconds regardless of the value of the pressure.

Gnam[10] has shown that there is a significant decrease in the heat transfer coefficient in dropwise condensation as the pressure of the vapor is decreased. The above results indicate that the decrease in the heat transfer coefficient is a manifestation of the slower growth of individual drops at lower pressures.

4.4 Effect of Contact Angle

The analytical results obtained in the case of hemispherical drops may be extended, in an approximate manner, to include contact angles other than 90°. Referring to Fig. 17, the drop is now assumed to be a spherical segment of base diameter D, contact angle θ, and radius of curvature r. The liquid-vapor interface is assumed to be uniformly at its average temperature T_{ia}. A is the area of the interface, B is the base area, and V is the volume of the drop. From geometry

$$
\begin{aligned}
D &= 2r \sin\theta \\
A &= 2\pi r^2 (1-\cos\theta) \\
B &= \pi r^2 \sin^2\theta \\
V &= \tfrac{1}{3}\pi r^3 (1-\cos\theta)^2 (2+\cos\theta)
\end{aligned}
\qquad (21)
$$

The heat transferred through the drop may be expressed alternately as

$$
q_d = h_e A (T_v - T_{ia}) \equiv h_d B (T_{ia} - T_s) \qquad (22)
$$

where the second equation defines h_d, the drop heat transfer coefficient. Using Eqs. 21 and 22

$$\frac{T_{ia}-T_s}{T_v-T_s} = \frac{1}{1+\dfrac{T_v-T_{ia}}{T_{ia}-T_s}} = \frac{1}{1+\dfrac{1+\cos\theta}{2}\dfrac{h_d}{h_e}} \tag{23}$$

Total energy transferred to a drop of contact angle θ and radius of curvature r is

$$Q = \rho_l V \lambda = \frac{1}{3}\pi \rho_l \lambda (1-\cos\theta)^2(2+\cos\theta) r^3$$

Differentiating with respect to time

$$\frac{dQ}{dt} = q_d = \pi \rho_l \lambda (1-\cos\theta)^2(2+\cos\theta) r^2 \frac{dr}{dt} \tag{24}$$

Eqs. 22, 23, and 24 are combined to give

$$\frac{dr}{dt} = \frac{(1+\cos\theta)(T_v-T_s)}{(1-\cos\theta)(2+\cos\theta)\rho_l \lambda} \frac{h_d}{1+\dfrac{1+\cos\theta}{2}\dfrac{h_d}{h_e}} \tag{25}$$

Before Eq. 25 can be integrated, an expression for h_d must be found. McCormick and Baer[17] have used a conformal mapping technique to show that

$$\frac{D h_d}{k_\ell} = \frac{8}{\theta} \int_0^{D/2} \frac{x\,dx}{(D/2)^2 - x^2}$$

Because of the assumption that the liquid-vapor interface is at a uniform temperature, there is a discontinuity at the base periphery where the interface touches the wall. Hence, the integral above has a singularity at $x = D/2$. McCormick and Baer suggest that the integral be evaluated between $x = 0$ and $x = CD/2$ for $C < 1$, so that

$$\frac{D h_d}{k_\ell} = \frac{4}{\theta} \ln \frac{1}{1 - C^2} \tag{26}$$

This amounts to using less than the total base area of the drop and, in effect, tends to correct for the assumption that the interface temperature is uniform. C^2 in Eq. 26 is the fraction of the base area to be used. It is not clear, however, what value should be assigned to it. In the case of hemispherical drops an expression for h_d can readily be found from Eqs. 14 and 15 of section 4.2. The result is

$$\left(\frac{D h_d}{k_\ell}\right)_{\theta = 90^\circ} = 4 \frac{\sum_{\substack{m=1 \\ \text{odd}}}^{\infty} \frac{m(2m+1)}{1 + \frac{k_\ell}{h_e r} m} \left[\int_0^1 P_m(x)\,dx\right]^2}{\sum_{\substack{m=1 \\ \text{odd}}}^{\infty} \frac{2m+1}{1 + \frac{k_\ell}{h_e r} m} \left[\int_0^1 P_m(x)\,dx\right]^2}$$

the right hand side of which is plotted in Fig. 18 against $k_\ell / h_e r$. Results of using Eq. 26 with different fractions of the base area are also indicated. If $k_\ell / h_e r$ is not much smaller than 0.1, Dh_d/k_ℓ is fairly well approximated by Eq. 26 when C^2 in that equation is taken to be 0.9, so that

$$\frac{Dh_d}{k_\ell} \approx \frac{9.2}{\theta} \equiv f(\theta) \tag{27}$$

It is now assumed that Eq. 27 applies not only to hemispherical drops but also to drops having contact angles other than 90°, with the understanding that the validity of this assumption becomes increasingly doubtful as the contact angle deviates from 90°.

Substituting for h_d from Eq. 27, and for h_e from Eq. 20, into Eq. 25

$$\left[r + \frac{(1+\cos\theta) f(\theta)}{4 \sin\theta} f(S) \frac{r}{r - r^*} \right] \frac{dr}{dt} = \frac{k_\ell (T_v - T_s)}{2 \rho_\ell \lambda} \frac{\sin\theta \, f(\theta)}{(1-\cos\theta)^2 (2+\cos\theta)}$$

Integrating between the limits $t = 0$, $r = r_o$, and t, r

$$t = \frac{\rho_\ell \lambda}{k_\ell (T_v - T_s)} f_1(\theta) \left\{ r^2 - r_o^2 + f_2(\theta) f(S) \left[r - r_o + r^* \ln \frac{r - r^*}{r_o - r^*} \right] \right\} \tag{28}$$

where

$$f_1(\theta) = \frac{(1-\cos\theta)^2(2+\cos\theta)}{\sin\theta f(\theta)}$$

$$f_2(\theta) = \frac{(1+\cos\theta)\, f(\theta)}{2\sin\theta}$$

$$f(S) = \left(\frac{2-\gamma}{2\gamma}\right)\left(\frac{2\pi}{g}\right)^{1/2} \frac{k_g R^{3/2} T_v^{5/2}}{\lambda^2 P_v^*}$$

Eq. 28 was used to calculate drop growth for contact angles 75°, 90°, and 105°. The results are plotted in Fig. 19. As might be expected, growth rate decreases as the contact angle is increased. The dotted line in the figure is the more accurate result obtained by using Eq. 17 of Section 4.2.

5. SUMMARY AND CONCLUSIONS

An examination of surface phenomena shows that with a spreading liquid net condensation occurs on a surface with any amount of relative supersaturation of the vapor. With a non-spreading liquid, there is a critical film thickness such that any film having a thickness smaller than critical evaporates; a film cannot spontaneously develop on the surface even with large relative supersaturation of the vapor.

The experimental observations indicate that no film greater than a monolayer in thickness develops on the surface as the surface is cooled to below the vapor temperature, and that as drops roll off the surface they do not leave films of liquid behind them.

The above results, together with the knowledge that a drop in order to grow must have a radius greater than critical, lead to pits and grooves in the surface as the most probable drop nucleation sites.

A model for drop growth based on the assumption that heat is transferred through the drop by conduction, but without using the assumption that the liquid-vapor interface is at the vapor temperature, gives results that are compatible with experimentally observed drop growth rates. With this model, drop growth rate is shown to be a function of the vapor pressure.

The following conclusions are reached:

1. The area between the drops does not have a liquid film greater than a monolayer in thickness.

2. No net condensation takes place on the area between the drops. Therefore, nearly all the energy transferred to the cooling surface is transferred through the drops.

3. The most probable drop nucleation sites are wetted pits and grooves in the surface.

4. The growth rate of small drops is significantly dependent on the vapor pressure.

LIST OF SYMBOLS

A	area of the liquid-vapor interface of a drop
B	base area of a drop
D	base diameter of a drop
f_s	fraction of a surface covered with adsorbed molecules (unity when the surface is covered with a complete monolayer, or more than a monolayer)
g	gravitational constant
h_d	drop heat transfer coefficient
h_e	equivalent heat transfer coefficient at the liquid-vapor interface
I_m	intensity of reflected light along the initial (zero film thickness) minor axis of the ellipse of polarization
I_t	total intensity of reflected light
K_2	absorbtion index (optics)
k_ℓ	thermal conductivity of the liquid
ℓ	lateral height of liquid inside a pit
M	total mass
n_o, n_1, n_2	indices of refraction
P^*	saturation pressure
P_i^*	saturation pressure corresponding to the temperature of the liquid-vapor interface
P_i^{**}	equilibrium pressure corresponding to the temperature of the liquid-vapor interface
P_m	Legendre polynominals of the first kind
P_r^{**}	equilibrium pressure corresponding to drop radius of curvature
P_v	vapor pressure
P_v^*	saturation pressure corresponding to the vapor temperature
P_δ^{**}	equilibrium pressure corresponding to the thickness of a thin film

Q total energy transferred to a drop

q_d rate of heat transfer through a drop

R gas constant

R_p component of the electric vector of the reflected light parallel to the plane of incidence

R_s component of the electric vector of the reflected light perpendicular to the plane of incidence

r radius of curvature of a drop

r^* critical drop radius

r_o radius of curvature of a newly formed drop

r_p reflected to incident ratio of electric vector of light wave parallel to the plane of incidence

r_s reflected to incident ratio of electric vector of light wave perpendicular to the plane of incidence

T temperature

T_i temperature of the liquid-vapor interface

T_{ia} average temperature over the area of the liquid-vapor interface

T_s surface temperature

T_v vapor temperature

t time

V volume of a drop

v specific volume of the liquid

W work per unit area

w net rate of condensation per unit area

w_+ rate of condensation per unit area

w_- rate of evaporation per unit area

y phase retardation suffered by light travelling through a transparent film

α orientation angle of the ellipse of polarization

α_o orientation angle of the ellipse of polarization with zero film thickness

β ellipticity angle of the ellipse of polarization

β_o ellipticity angle of the ellipse of polarization with zero film thickness

γ condensation coefficient (fraction of molecules that strike a surface that condense)

Δ phase difference between the two components of the electric vector of a light wave

δ film thickness

δ^* critical film thickness

δ_o film thickness at which the net rate of mass transfer is zero

δ_p phase angle of R_p (optics)

δ_s phase angle of R_s (optics)

Z Gibbs potential

S Gibbs potential per unit mass

θ contact angle of a drop

Λ wavelength of light

λ latent heat of vaporization

λ_l energy per unit mass required to evaporate molecules from the liquid phase (approximately equal to the latent heat of vaporization)

λ_s energy per unit mass required to evaporate molecules from a surface

μ molecular diameter

ς radial distance from the center of a hemispherical drop

ς_l liquid density

σ surface tension; surface free energy per unit area

ϕ angle between a normal to the wall through the center of a hemispherical drop and any radial direction

ϕ_o, ϕ_1, ϕ_2 angles of incidence and refraction

ψ $\tan^{-1} R_p/R_s$ (optics)

ψ_c semi-cone angle of a conical pit

REFERENCES

1. Alty, T., and Mackay, C. A., Proceedings of the Royal Society A 149, 104, 1935.

2. Baer, E., and McKelvey, J. M., "Heat Transfer in Dropwise Condensation," Delaware Science Symposium, University of Delaware, 1958.

3. Blackman, L. C. F., Dewar, M. J. S., and Hampson, H., Journal of Applied Chemistry 7, 160, 1957.

4. Bobco, R. P., and Gosman, A. L., A.S.M.E. Paper No. 57-S-2, 1957.

5. Derjaguin, B. V., and Zorin, Z. M., Proceedings of the Second International Congress of Surface Activity, Vol. II, 145, Academic Press, 1957.

6. Emmons, H., A.I.Ch.E., Transactions 35, 109, 1939.

7. Eucken, A., Naturwissenschaften 25, 209, 1937.

8. Fatica, N., and Katz, D. L., Chemical Engineering Progress, Vol. 45, No. 11, 661, 1949.

9. Frenkel, J., "Kinetic Theory of Liquids," Dover, 1955.

10. Gnam, E., Forschungsheft 382, 17, 1937.

11. Hampson, H., and Ozisik, N., Institution of Mechanical Engineers, Proceedings, Vol. 1B, No. 7, 282, 1952.

12. Jakob, M., Mechanical Engineering 58, 738, 1936.

13. Keenan, J. H., "Thermodynamics," Wiley, 1957.

14. Langmuir, J., Journal of the American Chemical Society 40, 1361, 1918.

15. Langmuir, J., Chemical Reviews 19, 147, 1933.

16. McCormick, J. L., and Baer, E., Journal of Colloid Science 18, 208, 1963.

17. McCormick, J. L., and Baer, E., "Dropwise Condensation on Horizontal Surfaces," Department of Chemistry and Chemical Engineering, University of Illinois, 1962.

18. Osment, B. D. J., National Engineering Laboratory, Heat Division Paper No. 176, Glasgow, 1959.

19. Pruger, W., Zeitschrift fur Physik 115, 202, 1940.

20. Rothen, A., and Hanson, M., Review of Scientific Instruments 20, 66, 1949.

21. Schrage, R. W., "Interphase Mass Transfer," Columbia University Press, 1953.

22. Silver, R. S., and Simpson, H. C., "The Condensation of Superheated Steam," Proceedings of a Conference held at the National Engineering Laboratory, Glasgow, 1961.

23. Sugawara, S., and Michiyoshi, I., Memoirs of Faculty of Engineering, Kyoto University, Vol. 18, No. 2, 84, 1956.

24. Tammann, G., and Boehme, W., Annalen der Physik 5, 1935.

25. Topper, L., and Baer, E., Journal of Colloid Science 10, 225, 1955.

26. Tronstad, L., Transactions of the Faraday Society 31^2, 1151, 1935.

27. Vasicek, A., "Optics of Thin Films," North-Holland, 1960.

28. Welch, J. F., and Westwater, J. W., "Microscopic Study of Dropwise Condensation," Department of Chemistry and Chemical Engineering, University of Illinois, 1960.

FIGURES

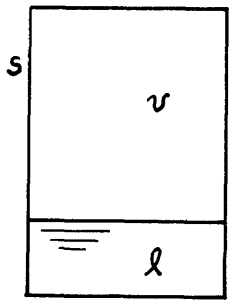

Fig. 1 Equilibrium between saturated vapor and solid surface

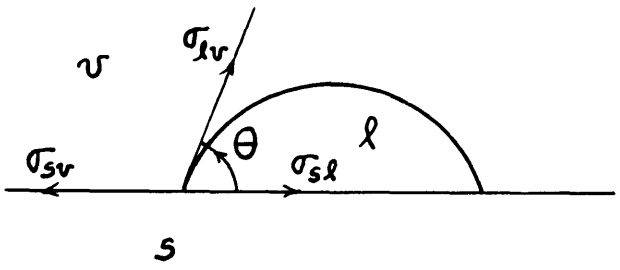

Fig. 2 Contact angle and surface energies

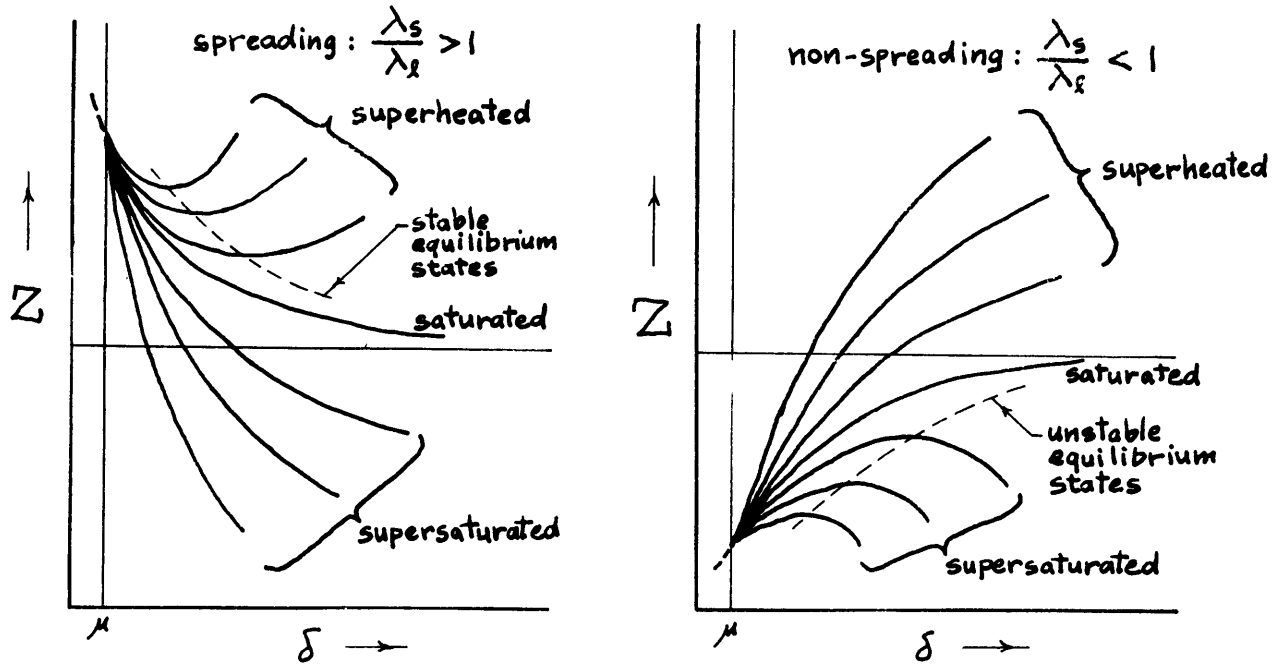

Fig. 3 Equilibrium states of a thin film

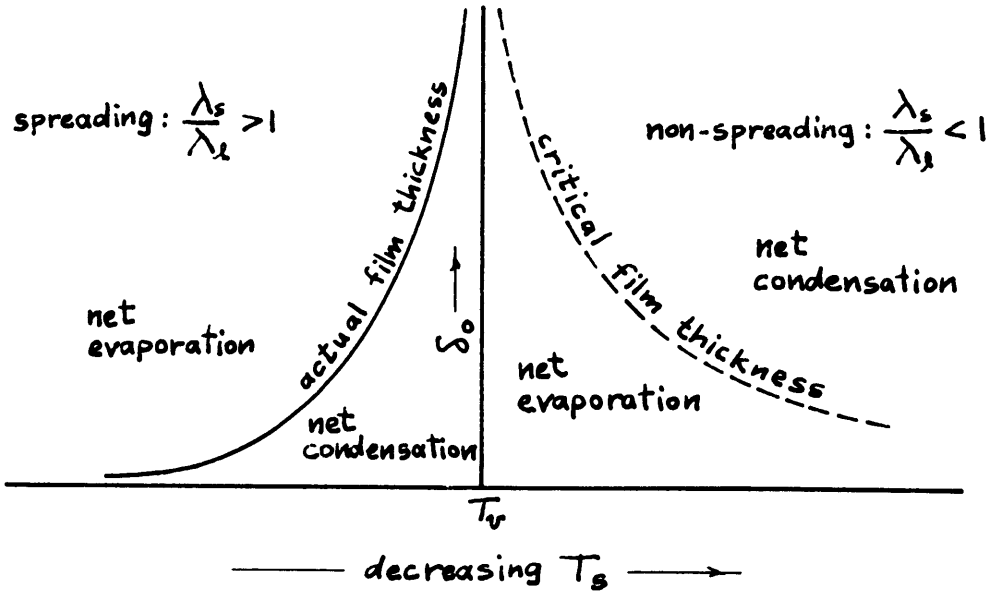

Fig. 4 Conditions for net condensation on a thin film

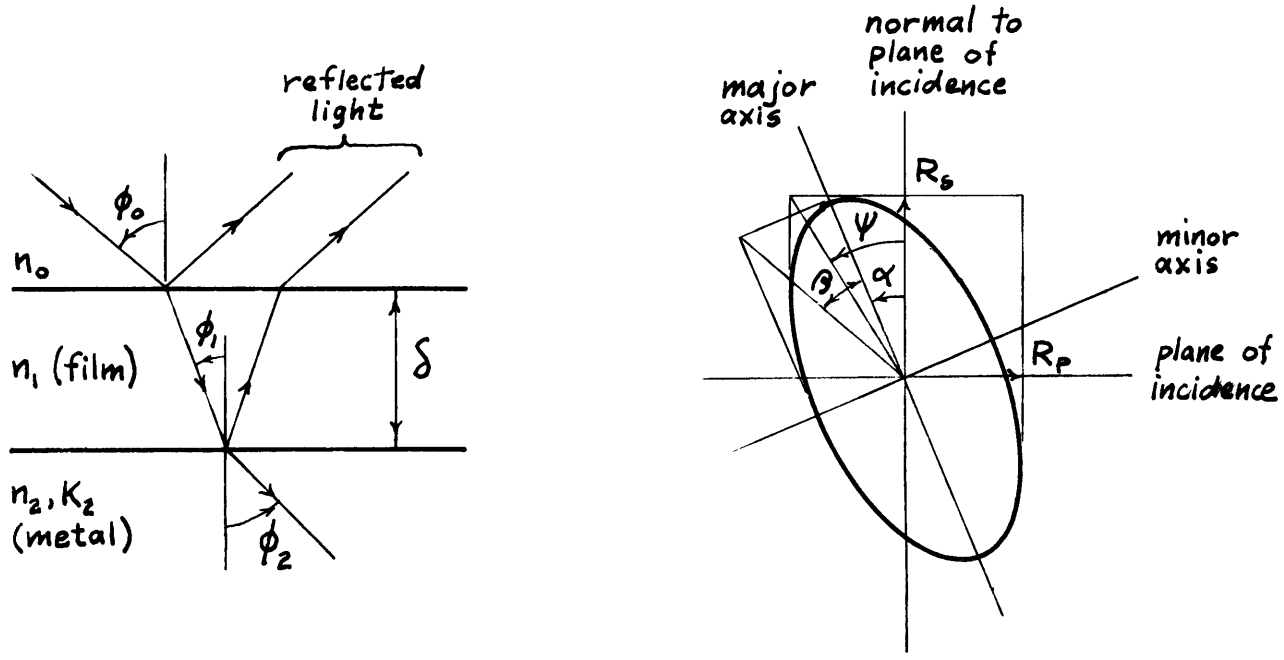

Fig. 5 (a) Reflection of light from a metal surface with a transparent film, (b) Polarization of the reflected light

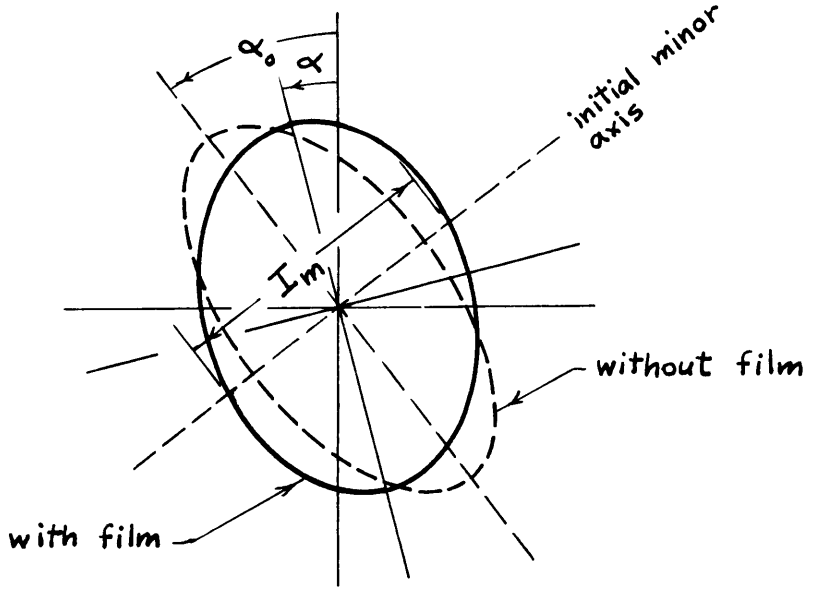

Fig. 6 Optical method used in the experiments

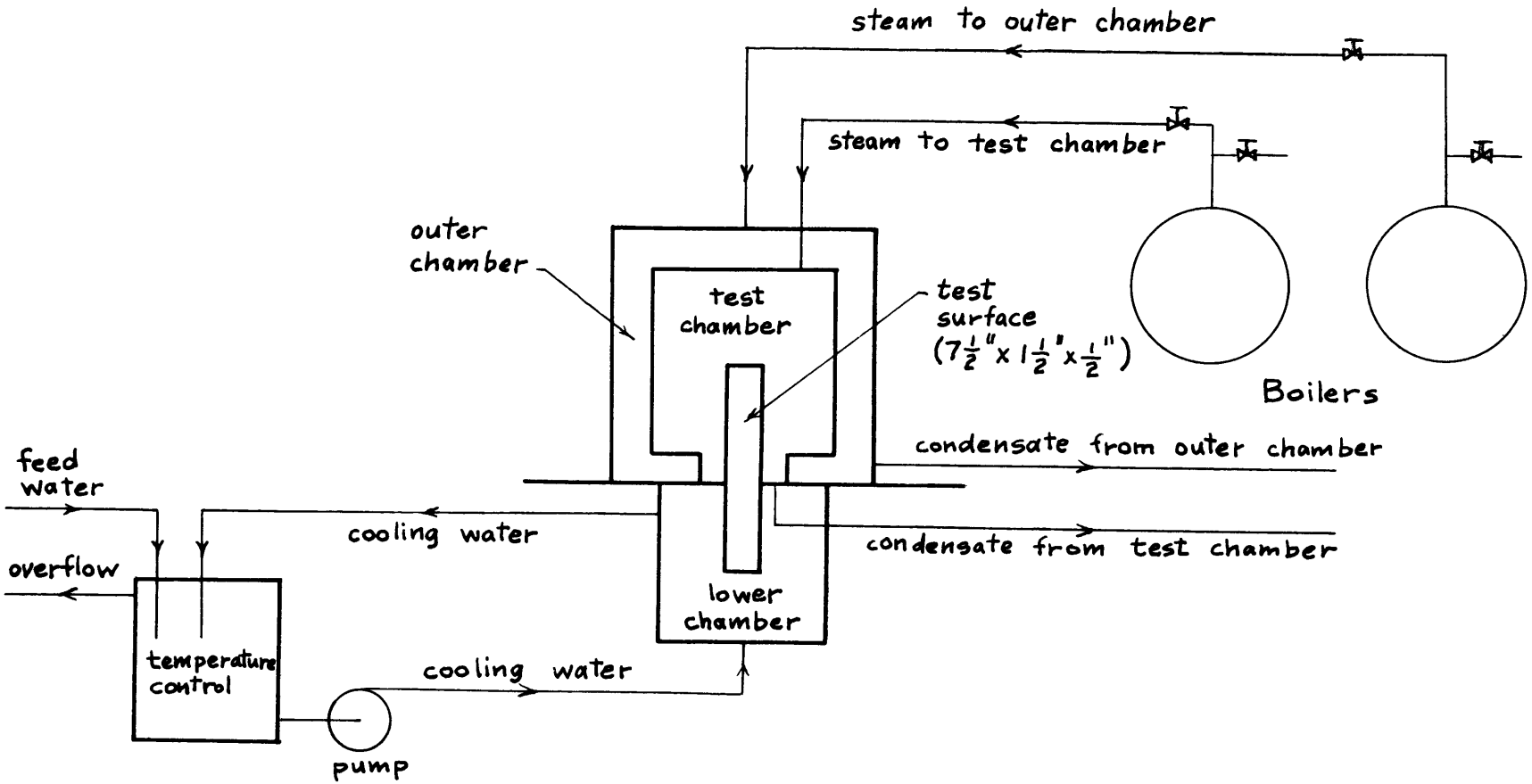

Fig. 7 Experimental arrangement (optical system not shown)

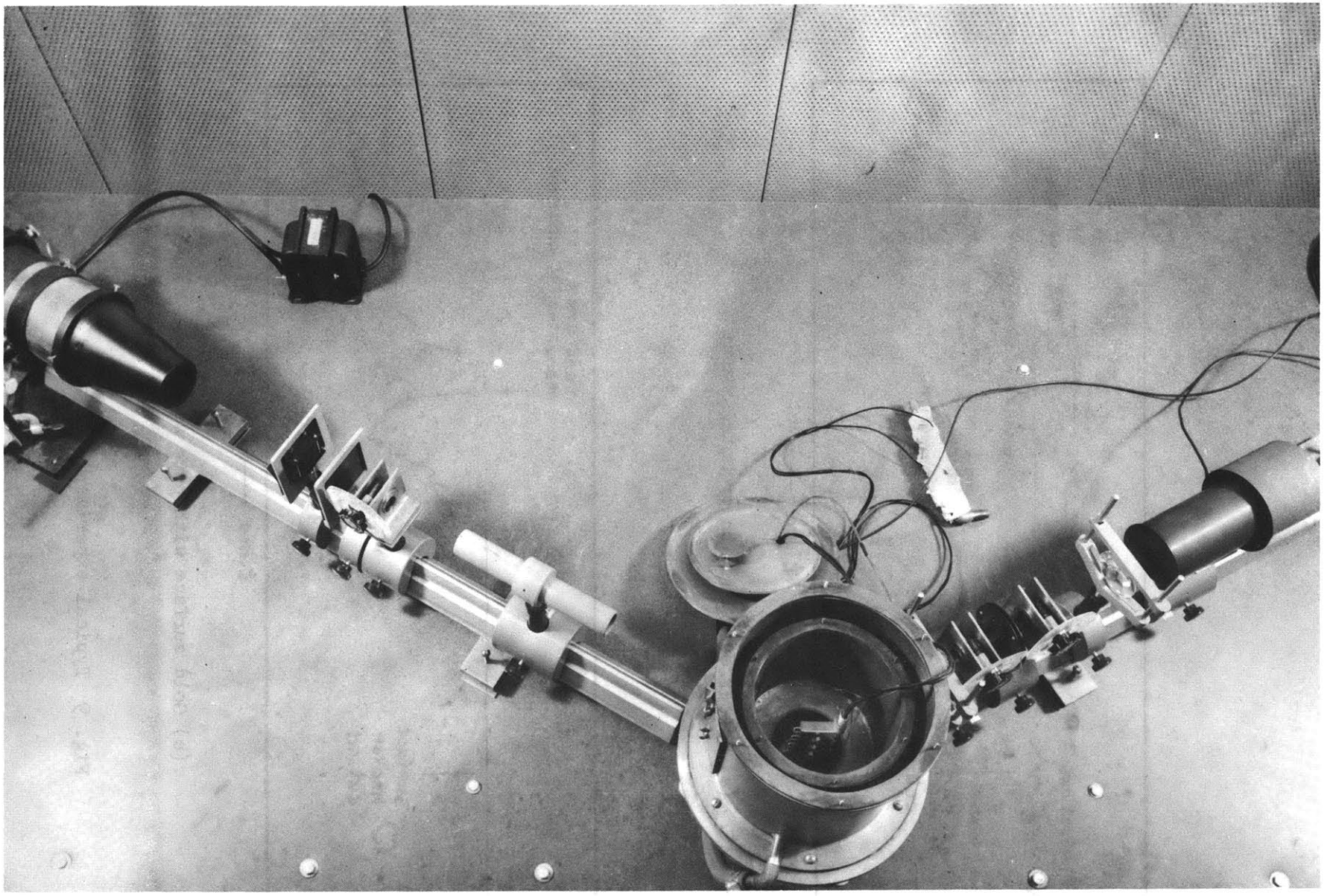

Fig. 8 Optical arrangement

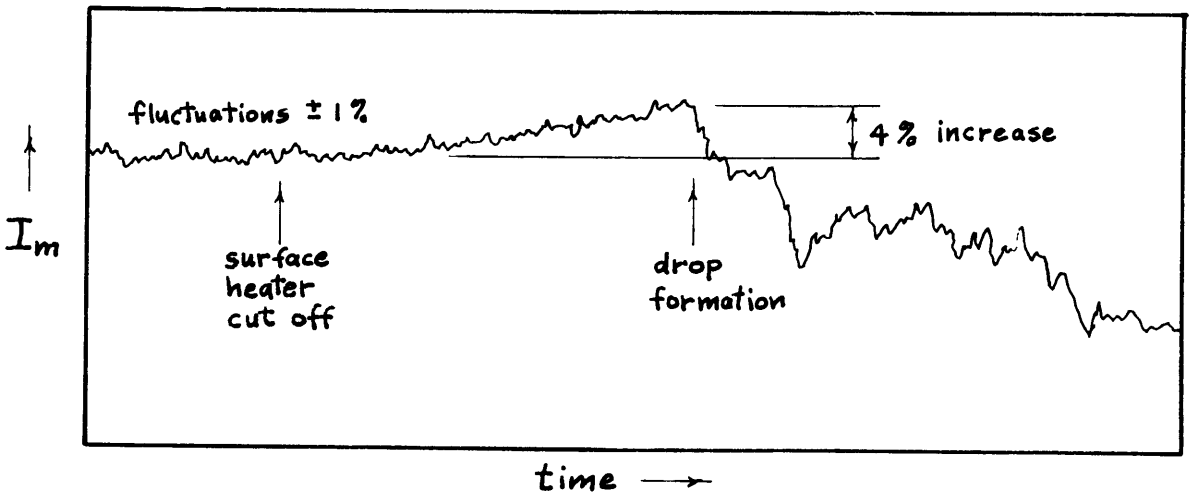

(a) Copper surface with promoted steam

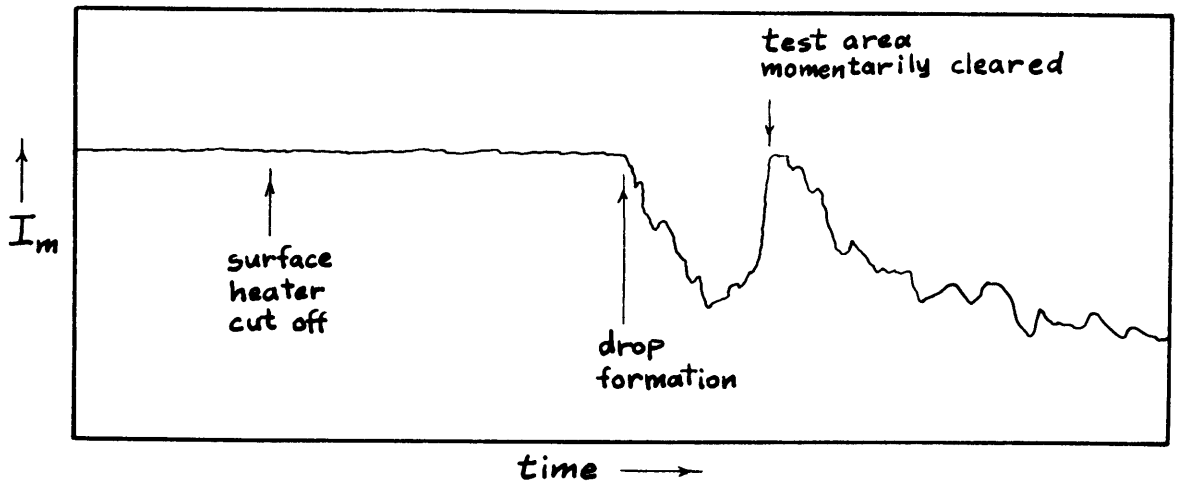

(b) Gold surface with pure steam

Fig. 9 Typical experimental results

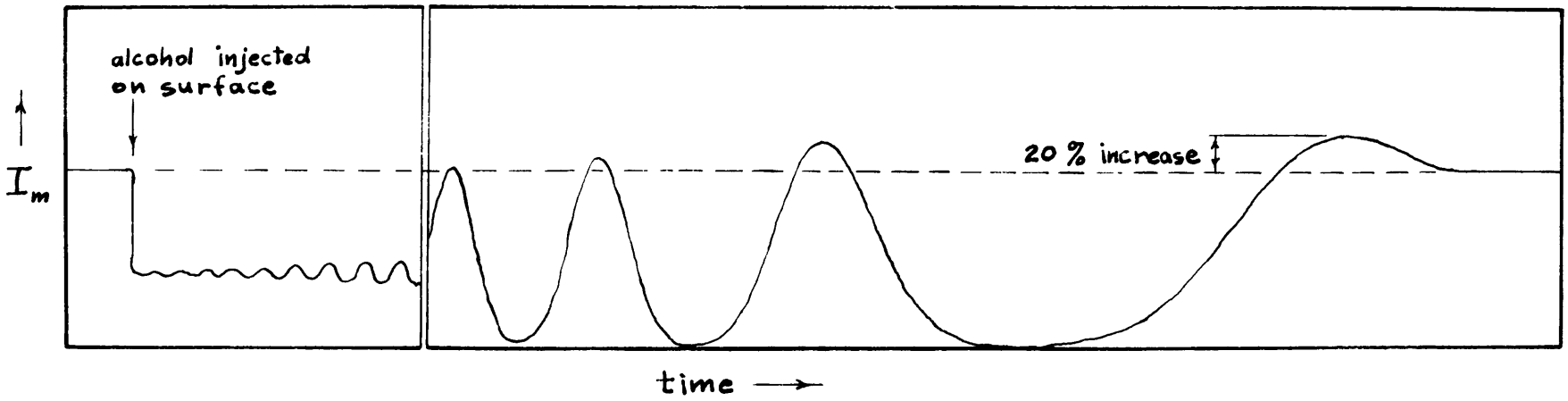

Fig. 10 Experimental variation of I_m with film thickness

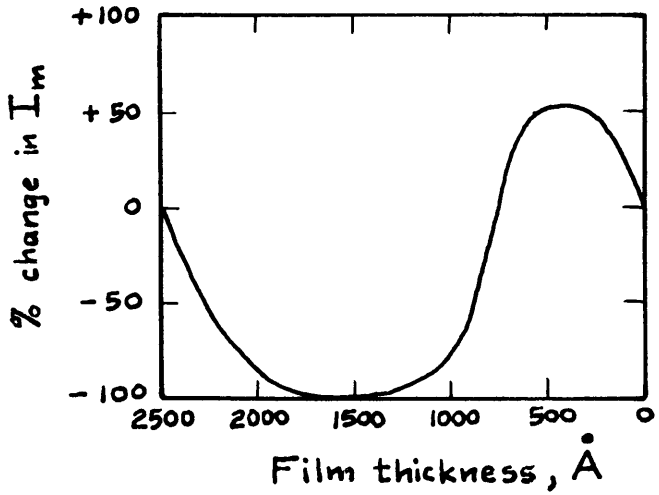

Fig. 11 Calculated variation of I_m with film thickness

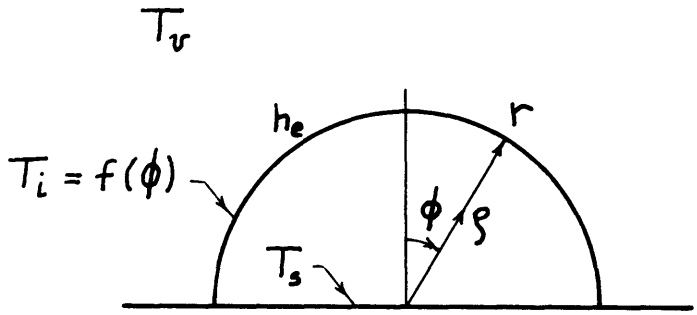

Fig. 12 Model for analyzing growth of hemispherical drops

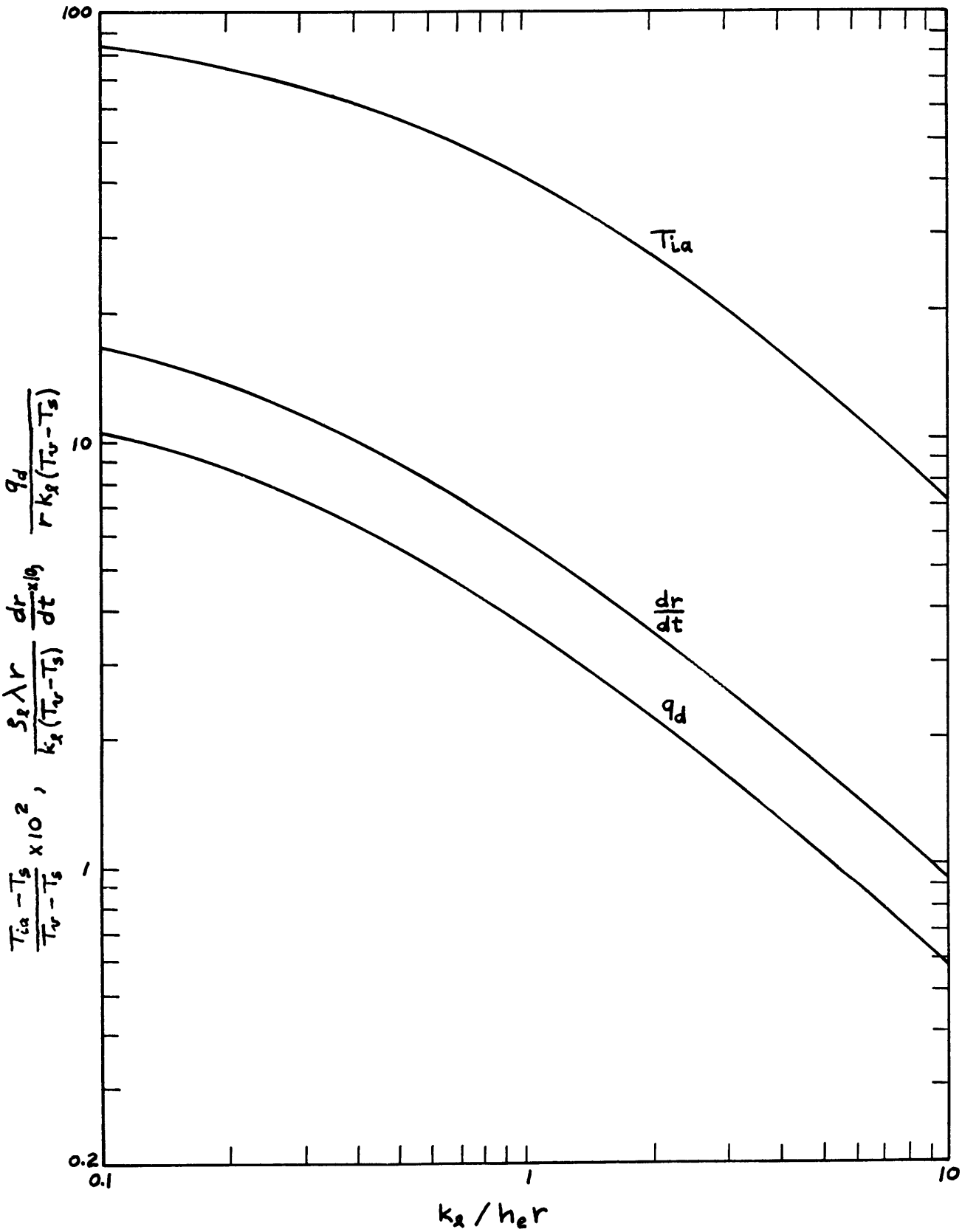

Fig. 13 Variation of average interface temperature, heat transfer through the drop, and rate of drop growth, with $k_\ell / h_e r$

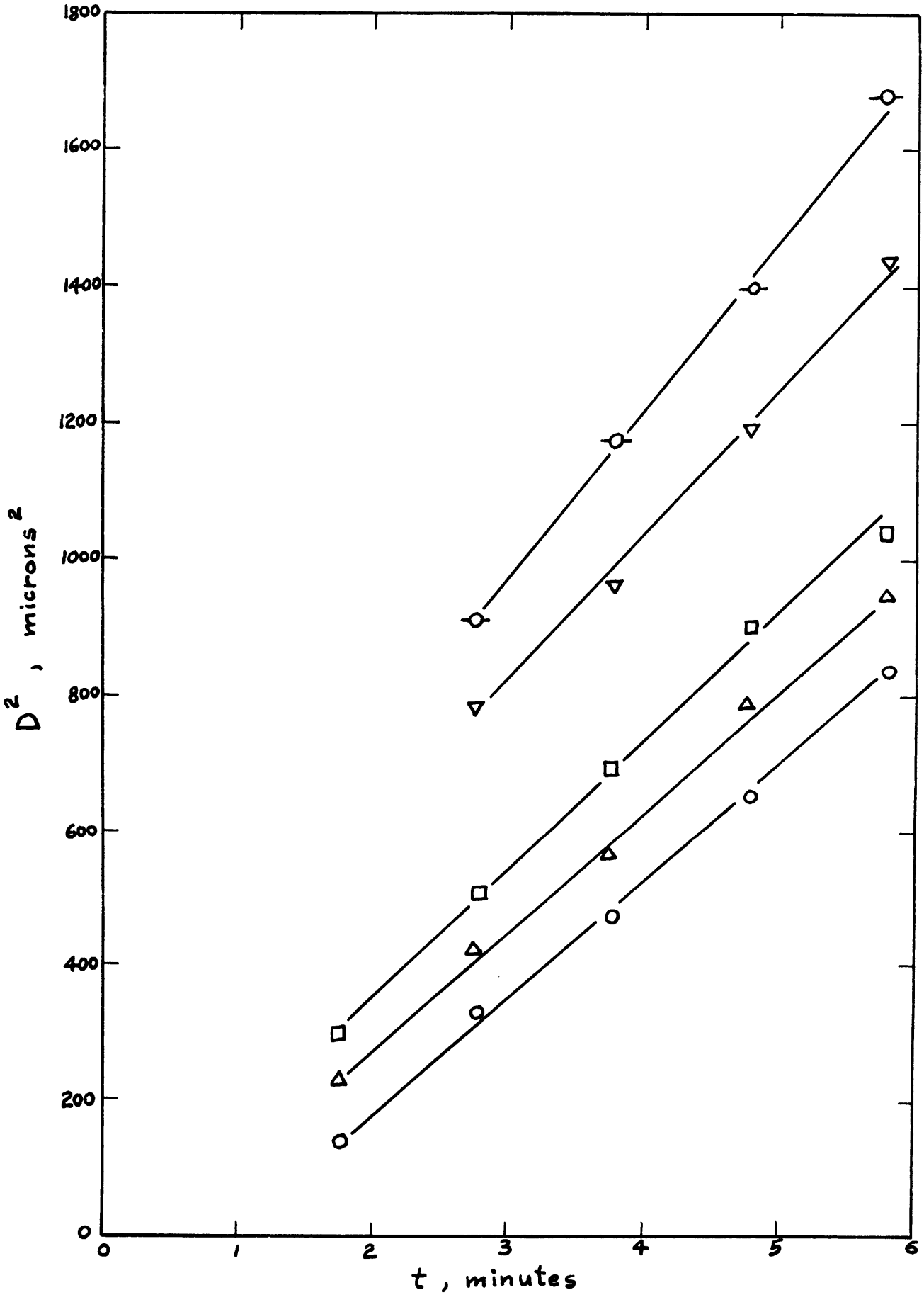

Fig. 14 Drop growth observed by McCormick and Baer

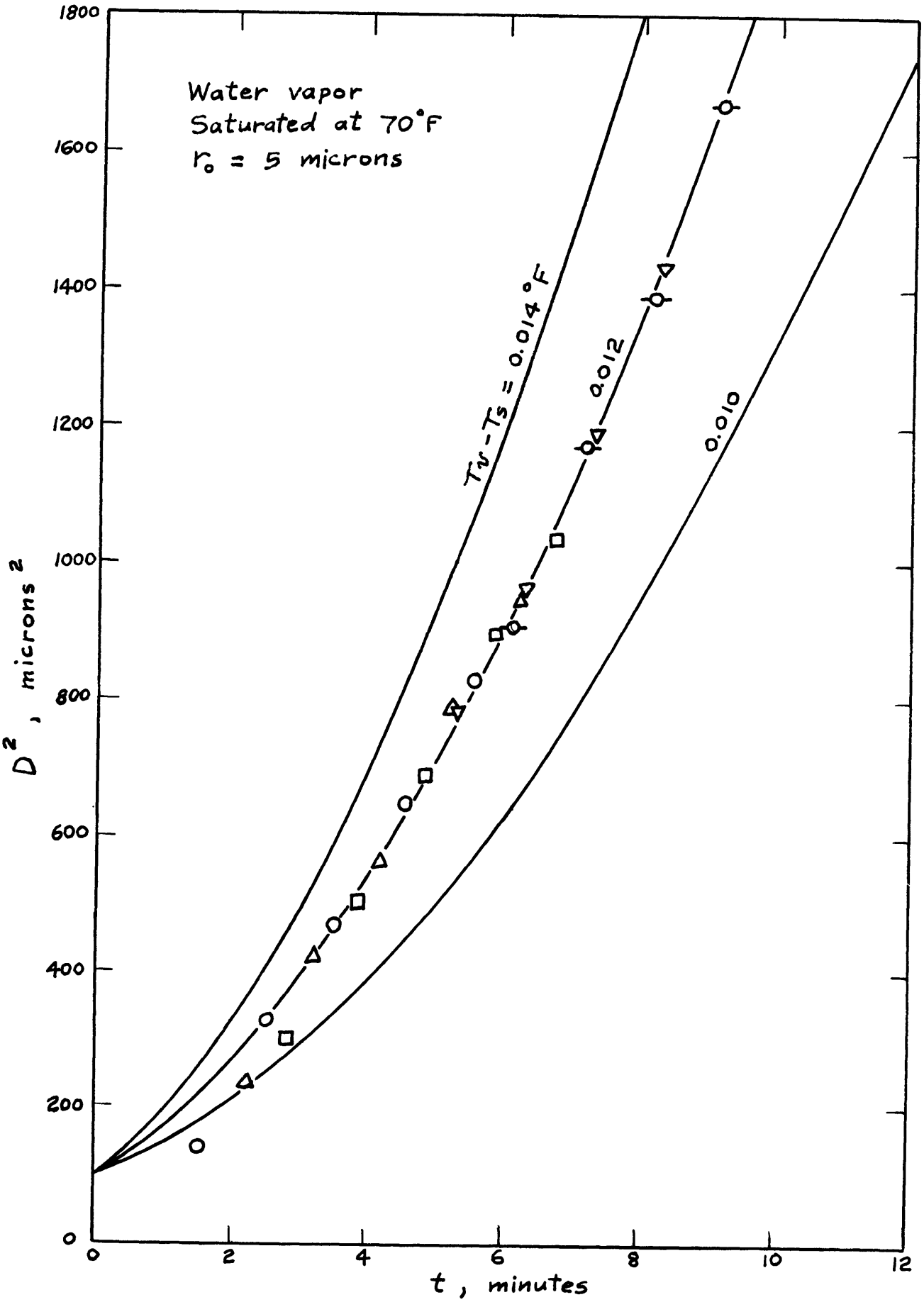

Fig. 15 Correlation of McCormick and Baer's data

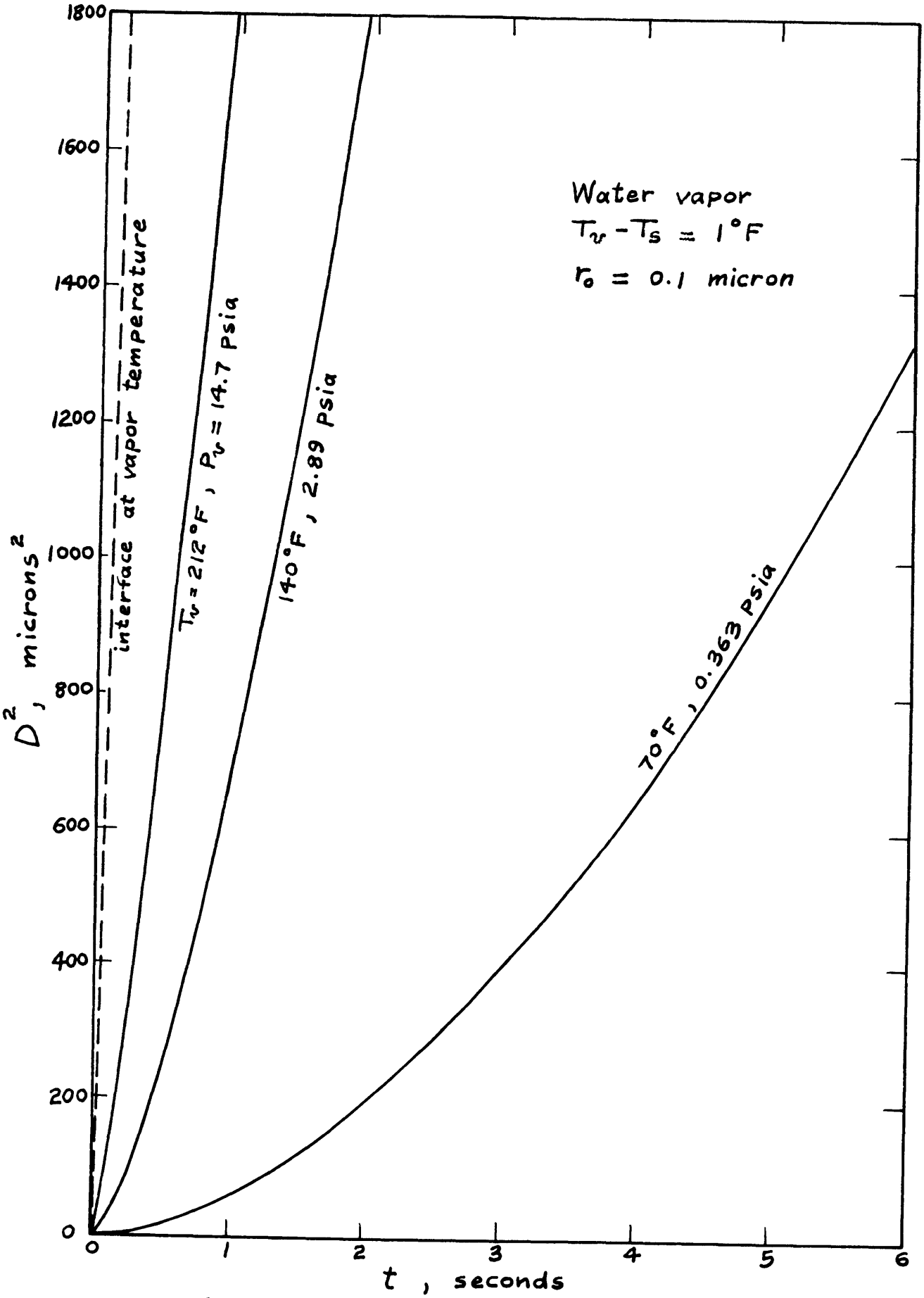

Fig. 16 Effect of pressure on drop growth rate

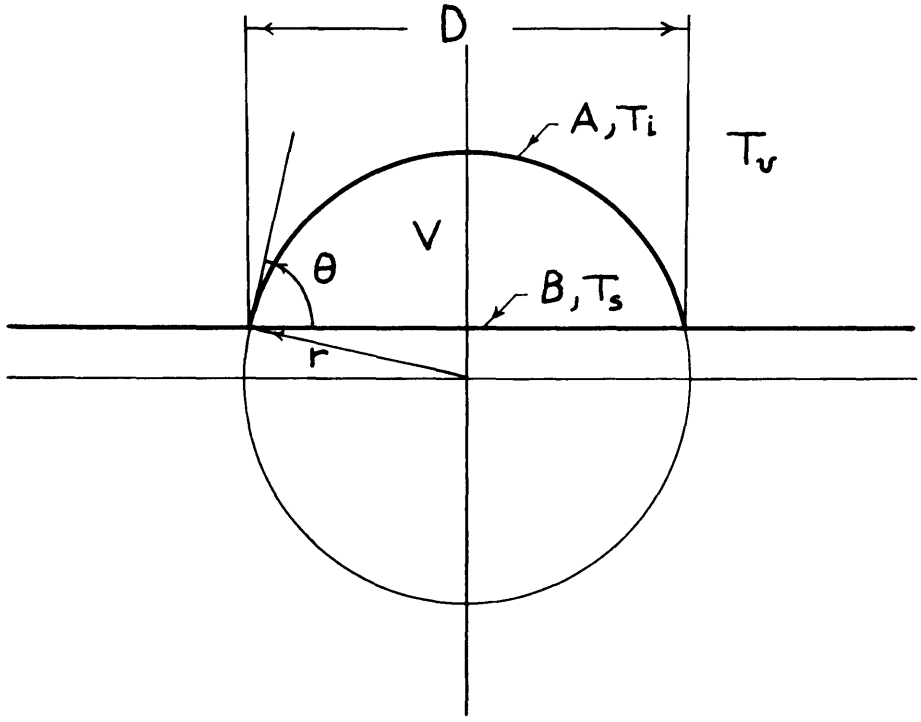

Fig. 17 Model with drop considered as a hemispherical segment

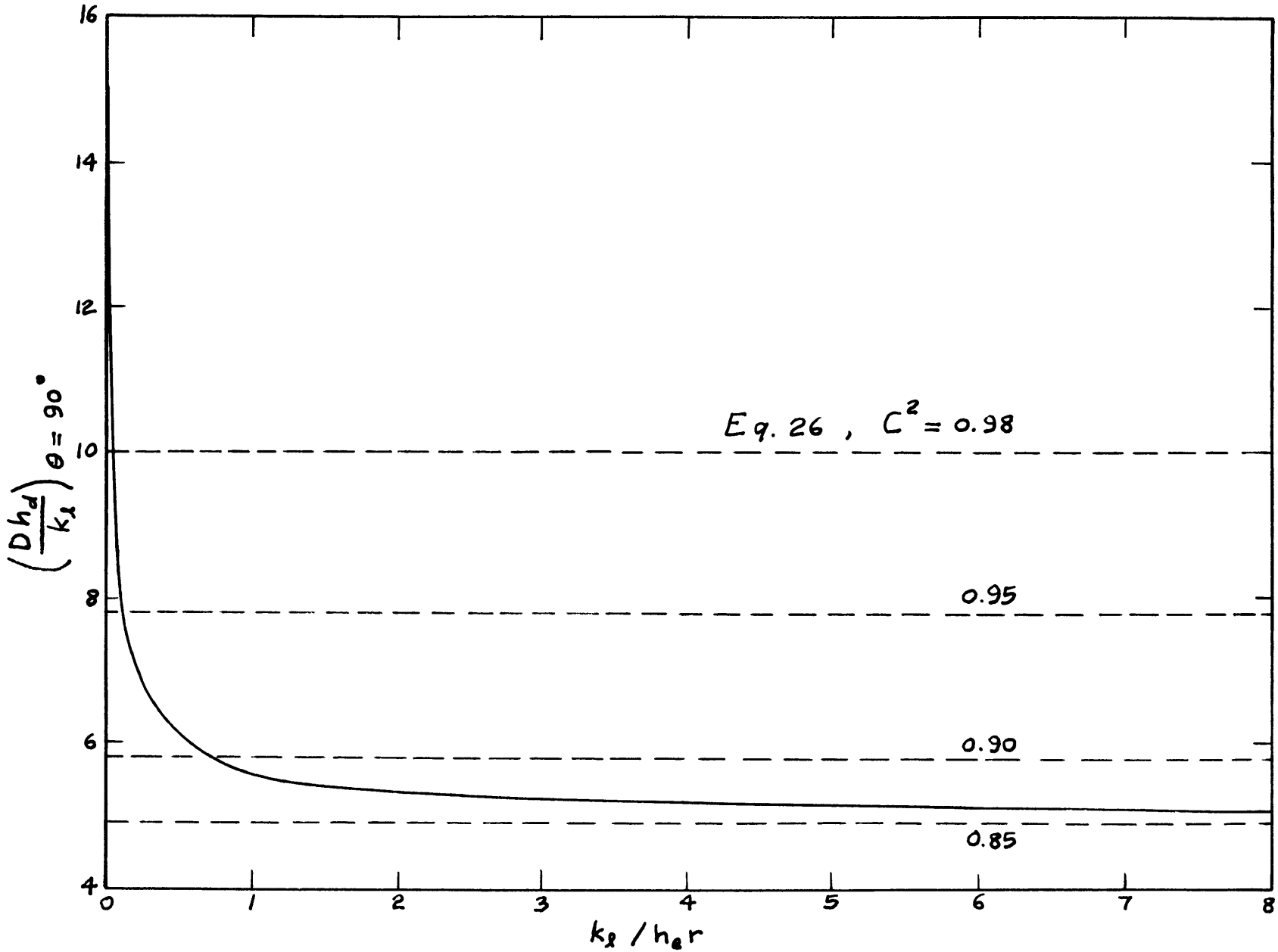

Fig. 18 Fraction of base area of drop to be used in conduction model

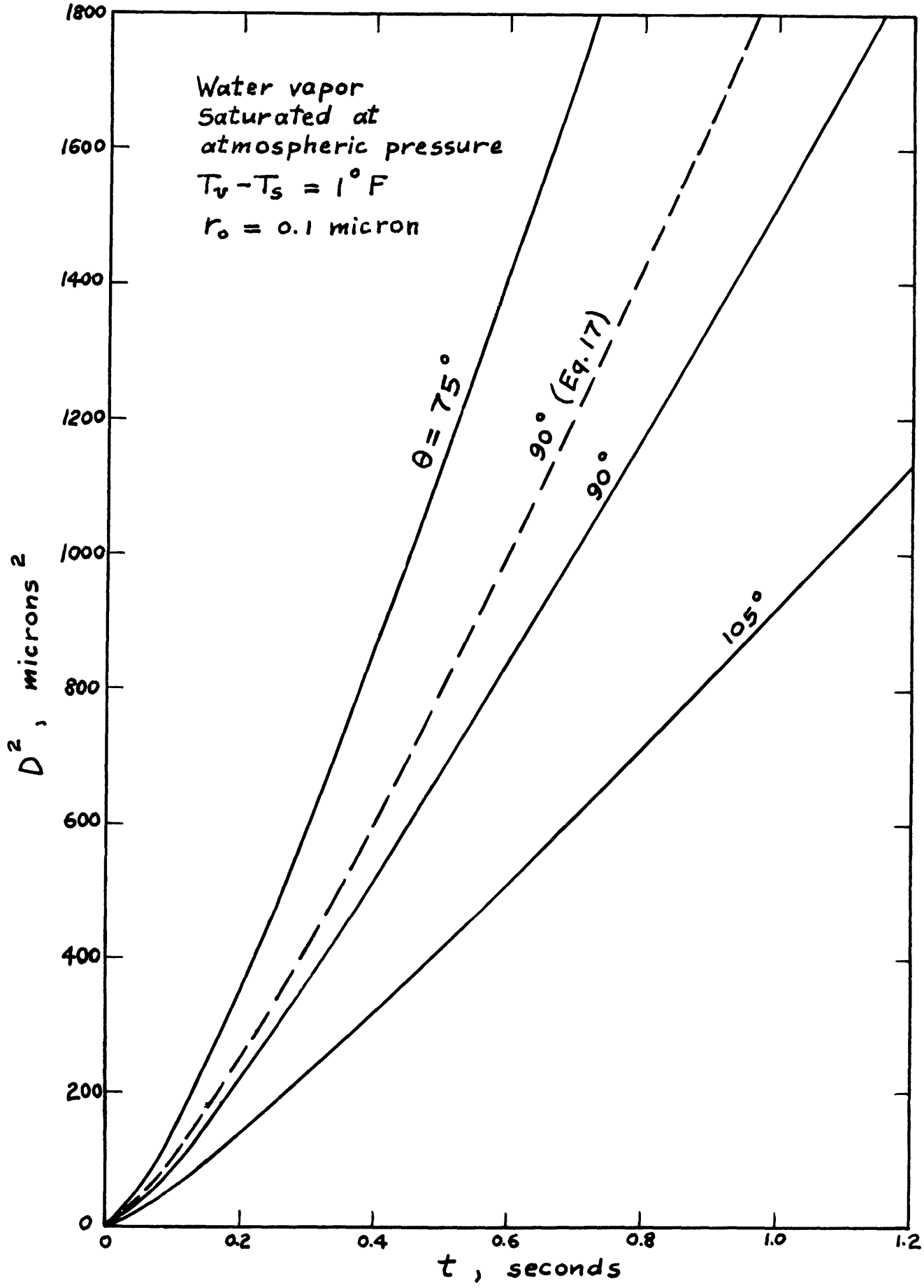

Fig. 19 Effect of contact angle on drop growth rate

APPENDIX A

Derivation of Frenkel's Equation

Consider the system, shown in Fig. A1, consisting of a vapor and a thin film on a solid surface. It is desired to find an expression for the Gibbs potential Z of the system as a function of the film thickness δ. If the solid surface is replaced by the liquid phase of the substance, the film becomes a true liquid phase, and the Gibbs potential of the system becomes

$$Z' = \zeta_l \frac{\delta}{v_l} + \zeta_v \left(M - \frac{\delta}{v_l} \right) \tag{A1}$$

where ζ_l and ζ_v are the Gibbs potentials per unit mass of liquid and vapor, respectively, v_l is the volume per unit mass of liquid, and M is the total mass contained in the system. Putting the solid surface back involves doing work on the system by an amount which is equal to the resulting increase in the Gibbs potential of the system, so that

$$Z = Z' - W \tag{A2}$$

where W is the work done on the system. If entropy effects are neglected, the work done is equal to the increase in the energy of evaporation of the molecules in the film. Therefore

$$W = \int_{\mu}^{\delta} \lambda_{sx} \frac{dx}{v_l} - \lambda_l \frac{\delta}{v_l} \qquad \text{(A3)}$$

where μ is the molecular diameter, λ_{sx} is the evaporation energy per unit mass of molecules on the outer surface of the film at a distance x from the solid surface, and λ_l is the evaporation energy per unit mass from the true liquid phase. The first term on the right hand side of Eq. A3 represents the energy of evaporation of all the molecules in the film, while the second term is the energy of evaporation of an equal number of molecules from the true liquid phase. λ_{sx} can be espressed as

$$\lambda_{sx} = \lambda_l - \lambda_{l,x} + \lambda_{s,x} \qquad \text{(A4)}$$

where $\lambda_{l,x}$ and $\lambda_{s,x}$ are the evaporation energies per unit mass of molecules a distance x away from the liquid and from the solid surface, respectively. The meaning of Eq. A4 is graphically represented in Fig. A2. From a consideration of molecular forces, Frenkel obtains the following approximate relations

$$\frac{\lambda_{l,x}}{\lambda_l} = \frac{\lambda_{s,x}}{\lambda_s} = \frac{\mu^3}{x^3}$$

with the use of which, Eq. A4 becomes

$$\frac{\lambda_{sx}}{\lambda_l} = 1 - \left(1 - \frac{\lambda_s}{\lambda_l}\right)\frac{\mu^3}{x^3}$$

which is used to integrate Eq. A3, giving

$$W = \frac{\lambda_l}{2v_l}\left[\left(1 - \frac{\lambda_s}{\lambda_l}\right)\frac{\mu^3}{\delta^2} - \left(3 - \frac{\lambda_s}{\lambda_l}\right)\mu\right]$$

which is combined with Eqs. A1 and A2, giving the final result

$$Z = \frac{S_l - S_v}{v_l}\delta + \frac{\lambda_s - \lambda_l}{2v_l}\frac{\mu^3}{\delta^2} + \left[\frac{(3\lambda_l - \lambda_s)\mu}{2v_l} + S_v M\right]$$

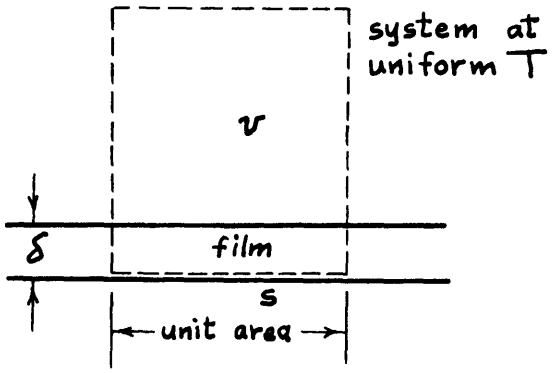

Fig. A1

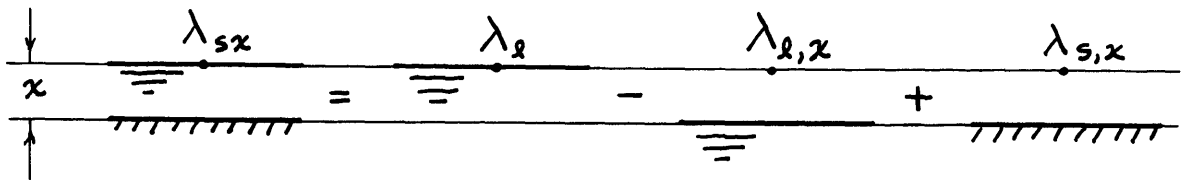

Fig. A2

APPENDIX B

Derivation of Eq. 10 of Section 3.2

Symbols used below are the same as in Chapter 3. Referring to Fig. 6, the components of R_p and R_s in the plane of the initial minor axis are $R_p \cos \alpha_o$ and $R_s \sin \alpha_o$. They are out of phase with respect to one another by an angle Δ , so that the two waves in this plane are

$$y_p = R_p \cos \alpha_o \sin(\omega t)$$

$$y_s = -R_s \sin \alpha_o \sin(\omega t + \Delta)$$

The square of the resultant amplitude of the two waves above is the intensity I_m along the initial minor axis, so that

$$I_m = R_p^2 \cos^2 \alpha_o + R_s^2 \sin^2 \alpha_o - 2 R_p R_s \sin \alpha_o \cos \alpha_o \cos \Delta$$

which, with the use of trigonometric relations, becomes

$$I_m = \frac{1}{2}\left(R_p^2 + R_s^2\right) + \frac{1}{2}\left(R_p^2 - R_s^2\right) \cos 2\alpha_o - R_p R_s \sin 2\alpha_o \cos \Delta \qquad \text{(B1)}$$

Defining the symbol ε by the following equation

$$\varepsilon \equiv \alpha_o - \alpha$$

and substituting for α_o into Eq. B1, gives

$$I_m = \frac{1}{2}\left(R_p^2 + R_s^2\right) + \cos 2\varepsilon\left[\frac{1}{2}\left(R_p^2 - R_s^2\right)\cos 2\alpha - R_p R_s \sin 2\alpha \cos\Delta\right]$$

$$-\sin 2\varepsilon\left[\frac{1}{2}\left(R_p^2 - R_s^2\right)\sin 2\alpha + R_p R_s \cos 2\alpha \cos\Delta\right] \qquad (B2)$$

The following relations exist between α , β , ψ , and Δ (see Vasicek[27])

$$\cos\Delta = \frac{\tan 2\alpha}{\tan 2\psi}$$

$$\cos 2\alpha = \frac{\cos 2\psi}{\cos 2\beta} \qquad (B3)$$

Also, from the definition of ψ

$$\tan\psi \equiv \frac{R_p}{R_s}$$

the following relations are obtained

$$\tan 2\psi = -\frac{2R_p R_s}{R_p^2 - R_s^2}$$

$$\cos 2\psi = -\frac{R_p^2 - R_s^2}{R_p^2 + R_s^2} \qquad \text{(B4)}$$

Using Eqs. B3 and B4, Eq. B2 becomes

$$I_m = \frac{1}{2}\left(R_p^2 + R_s^2\right)\left(1 - \cos 2\beta \cos 2\epsilon\right)$$

and, after replacing $\alpha_o - \alpha$ for ϵ, and noting that $R_p^2 + R_s^2$ is equal to the total light intensity I_t, the final result is obtained

$$\frac{I_m}{I_t} = \frac{1}{2}\left[1 - \cos 2\beta \cos 2(\alpha_o - \alpha)\right]$$

APPENDIX C

Procedure for Relating I_m to the Film Thickness

All equations given below, except the one derived in Appendix B, can be found in Vasicek[27]. The numerical example is for the set of conditions shown in Fig. C1.

The optical constants $\bar{n}_2$ and $\bar{K}_2$ of the metal surface are for normal incidence of light. Their values for angle of incidence ϕ_1 may be calculated from

$$n_2^2 = \frac{1}{2}\left[\left(E'^2 + F'^2\right)^{1/2} + E'\right]$$

$$K_2 = \left[1 - \frac{E}{n_2^2}\right]^{1/2}$$

where

$$E' = E + n_o^2 \sin^2 \phi_o$$

$$F' = \left(F^2 - 4E\, n_o^2 \sin^2 \phi_o\right)^{1/2}$$

$$E = \bar{n}_2^2 \left(1 - \bar{K}_2^2\right)$$

$$F = 2\, \bar{n}_2^2\, \bar{K}_2$$

The angles ϕ_1 and ϕ_2 are calculated from

$$\sin \phi_1 = \frac{n_0}{n_1} \sin \phi_0$$

$$\cos^2 \phi_2 = 1 - \frac{n_0^2}{n_2^2} \sin^2 \phi_0$$

It is convenient to have the incident light polarized in a plane making an angle 45° with the plane of incidence. The two components of the incident light, in the plane of incidence and in the plane perpendicular to the plane of incidence, are then equal to one another. In this case, calculation of the two components of the electric vector of the reflected light, R_p and R_s, is not necessary. It is sufficient to calculate r_p and r_s, the ratio of reflected to incident magnitudes of the two components. For reflection from the surface of the film

$$r_p' = \frac{n_1 \cos \phi_0 - n_0 \cos \phi_1}{n_1 \cos \phi_0 + n_0 \cos \phi_1}$$

$$r_s' = \frac{n_0 \cos \phi_0 - n_1 \cos \phi_1}{n_0 \cos \phi_0 + n_1 \cos \phi_1}$$

For reflection from the metal surface, the phase angles of the two components δ_p'' and δ_s'' must be calculated as well as r_p'' and r_s''

$$r_p''^2 = \frac{(E\cos\phi_1 - n_1 n_2 \cos\phi_2)^2 + (F\cos\phi_1 - n_1 n_2 K_2)^2}{(E\cos\phi_1 + n_1 n_2 \cos\phi_2)^2 + (F\cos\phi_1 + n_1 n_2 K_2)^2}$$

$$r_s''^2 = \frac{(n_1\cos\phi_1 - n_2\cos\phi_2)^2 + n_2^2 K_2^2}{(n_1\cos\phi_1 + n_2\cos\phi_2)^2 + n_2^2 K_2^2}$$

$$\tan\delta_p'' = \frac{2n_1\cos\phi_1 (E n_2 K_2 - F n_2 \cos\phi_2)}{(E^2+F^2)\cos^2\phi_1 - n_1^2(n_2^2\cos^2\phi_2 + n_2^2 K_2^2)}$$

$$\tan\delta_s'' = \frac{2n_1 n_2 K_2 \cos\phi_1}{n_1^2\cos^2\phi_1 - n_2^2\cos^2\phi_2 - n_2^2 K_2^2}$$

It should be noted that r_p'' and r_s'' are always taken as positive, whereas the signs of δ_p'' and δ_s'' are determined from the signs of the numerator and the denominator in their respective equations. If the numerator is considered as the sine of the angle and the denominator as the cosine, the

quadrant in which the angle must lie is fixed.

The two reflections are combined by using the following equations

$$r_p^2 = \frac{r_p'^2 + r_p''^2 + 2 r_p' r_p'' \cos(y - \delta_p'')}{1 + r_p'^2 r_p''^2 + 2 r_p' r_p'' \cos(y - \delta_p'')}$$

$$\tan \delta_p = \frac{- r_p''(1 - r_p'^2) \sin(y - \delta_p'')}{r_p'(1 + r_p''^2) + r_p''(1 + r_p'^2) \cos(y - \delta_p'')}$$

r_s and δ_s are determined by the same equations as above, with the subscripts changed to s. The phase retardation suffered as the light travels through the film appears in the above equations through y which is given by

$$y = \frac{4\pi}{\Lambda} n_1 \cos \phi_1 \delta$$

and is seen to be a function of the film thickness δ . The other properties of the reflected light are calculated from

$$\tan \psi = \frac{r_p}{r_s}$$

$$\Delta = \delta_p - \delta_s$$

$$\tan 2\alpha = \tan 2\psi \cos \Delta$$

$$\sin 2\beta = \pm \sin 2\psi \sin \Delta$$

For the method used in this investigation, the following were also calculated

$$\frac{I_m}{I_t} = \frac{1}{2}\left[1 - \cos 2\beta \cos(2\alpha - 2\alpha_o)\right]$$

$$\frac{I_t}{(I_t)_o} = \frac{r_p^2 + r_s^2}{(r_p^2 + r_s^2)_o}$$

$$\frac{I_m}{(I_t)_o} = \frac{I_m}{I_t} \frac{I_t}{(I_t)_o}$$

when the subscript o indicates that the value of the quantity corresponds to zero film thickness.

In the quantity $(I_m/I_t)_o$, only I_m varies with the film thickness, so that the desired relation between I_m and δ is obtained. As an example, the following numerical results are given for the conditions of Fig. C1

δ (Å)	$\frac{I_m}{(I_t)_o}$	% increase in I_m
0	0.1158	0
50	0.1293	11.7
100	0.1416	22.3
150	0.1532	32.3

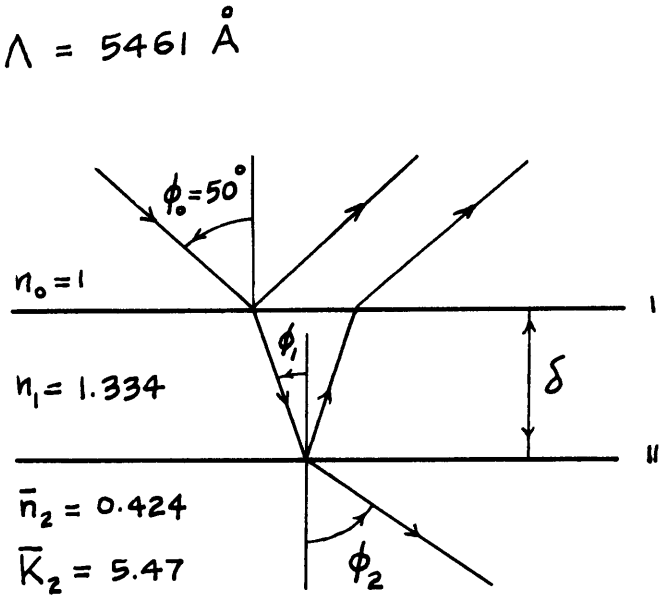

Thin film of water on gold

Fig. C1